DESIGN AND DEVELOPMENT OF A MICRO POWER, WATER CURRENT GENERATOR

A MAJOR QUALIFYING PROJECT REPORT
SUBMITTED TO THE FACULTY OF THE

WORCESTER POLYTECHNIC INSTITUTE

IN PARTIAL FULFILLMENT OF THE REQUIREMENTS FOR THE DEGREE OF BACHELOR OF SCIENCE IN ELECTRICAL AND COMPUTER ENGINEERING AND MECHANICAL ENGINEERING

_____

Ryan Bussett

_____

Christopher Chaggaris

_____

Michael O'Regan

_____

Andrew Turgeon

_____

Approved by Professor David Planchard, Primary Advisor

ABSTRACT

The goal of the project was to design and manufacture a scalable, liquid current power generator capable of harnessing energy contained in ocean currents for electrical applications. The project team utilized a coreless, direct drive, three phase axial-flux alternator driven by a pair of three-blade, diametrical flow Gorlov turbines. To develop the design, the group used several software products. DS SolidWorks was used to model design iterations for the machine. For the alternator design and analysis, a load-line analysis was done in MATLAB to allow easy modification during development. The group manufactured the machine using several resources, including two MakerBot Replicator 2 3D printers, several Haas CNC machines available in Washburn Shops, and multiple traditional open and hand machine tools. To test the machine, the group first analyzed the machine's power output at various speeds in a lab environment. Then, the device was ultimately run in the WPI Recreation Center Crew Tanks in order to effectively simulate the device in a submerged current flow scenario.

ACKNOWLEDGEMENTS

Our MQP team would like to thank the ME and ECE departments for continued academic support for our project. We would like to thank our primary advisor, Professor David Planchard, for his assistance with improving our design, rapid prototyping our hydrofoils, and for providing guidance throughout the project. Additionally, we would like to give a special thanks to our secondary ECE advisor, Professor Alexander Emanuel, for his assistance with improving the design of our alternator and for providing guidance throughout the project. Special thanks are given to BJA Magnetics, in Leominster MA, for providing us with our permanent magnets free of charge. The group would also like to acknowledge SkoDie for providing electrical steel laminations and the WPI rowing team for allowing our use of their training center as our testing location.

EXECUTIVE SUMMARY

The team assembled to complete a Major Qualifying Project consisted of two electrical engineering students, Ryan Bussett and Chris Chaggaris, as well as two mechanical engineering students, Andrew Turgeon and Mike O'Regan. As prospective engineers, we believe it is our shared responsibility to think about the major problems that face humanity. As such, all four members of our team shared a common interest in the advancement of renewable energy technologies. Global renewable energy consumption has risen steadily for the past several decades and, in the interest of developing more sustainable energy habits, humanity is investing more time and effort into wide varieties of renewable technologies. Hydro-power, solar absorption and wind-power technologies are some of the most recognizable areas of interest in this green revolution.

Upon looking into facilities and equipment available, the team decided on designing and developing a small-scale, hydropower generator device that could be scaled up and linked modularly, depending on application area geographical conditions. Having determined that water would be the renewable energy source of focus, the group sought to choose between capturing wave oscillations or flowing water current as a means of power production. It was determined that it would be advantageous to have a submerged device, as more volatile conditions typically exist at the surface of a water body, where a surface wave capturing device would be maintained. In addition, our institution, Worcester Polytechnic Institute, had just recently constructed a new sports and recreation center with a state-of-the-art, variable speed, crew rowing tank. The team saw this rowing tank as a valuable resource for thoroughly testing a fluid current conversion machine. With these conditions in mind, the team decided to focus our design to utilize flowing water to generate power, over wave power. Some anticipated applications of such a device include: installation of device(s) under coastal navigation buoys then linked together toward the bound for marina; suspension of device(s) from a boat to provide a mobile power source; installation of device(s) in a rivers, streams, or canals for focused flow capture; and or installation of device(s) on flow beds to be out of the way of surface activity.

The team spent the next several months doing background research into currently utilized methods and techniques for turbine technology, ocean current generators, ocean wave bobbers, as well as a variety of other energy conversion sources. Once the group became familiar with the operational aspects of the machines

currently being utilized, the development of design specifications began based on available resources, materials and manufacturing techniques, among other independent constraints. Before the preliminary solid modeling could occur, the group needed to define the scope of the project. The recent popularity of axial-flux alternator solutions for wind turbines has led to an increase in the research and development into the applications of this alternator topology. Correspondingly, it was determined that the project goal would be to produce a synchronous, direct-drive, axial-flux alternator to convert rotational energy of the turbine into electrical energy. The axial-flux topology has many potential benefits, particularly: no cogging torque, high power density and a high diameter to length ratio. Having discovered developments in liquid volume motion conversion regarded low-head hydrofoil turbines, the team decided to utilize a Gorlov vertical axis helical turbine for capturing the water current energy. An optimized hydrofoil profile was utilized for the turbine blades. After these factors had been set into place, the first stages of solid modeling and feature design began.

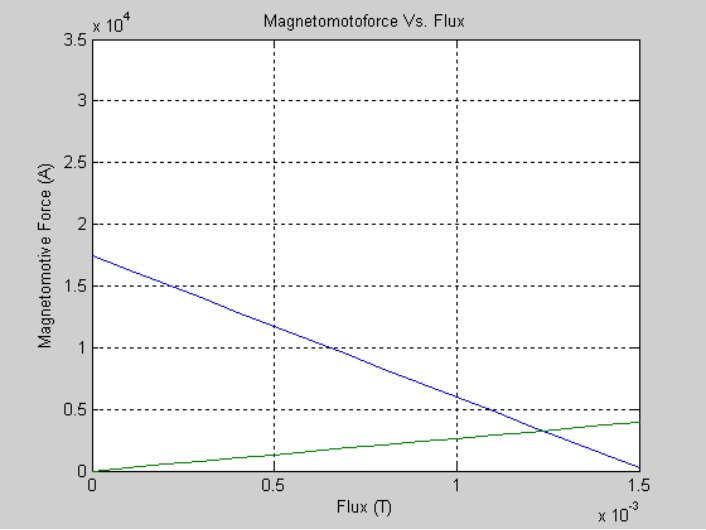

Figure 1: MATLAB Load-Line Analysis

In the design of the alternator, there were several variables that the team took into account. By simulating a load-line analysis in MATLAB (shown above in Figure 1), the team was able to modify the design on the fly and easily understand the effects of the modifications. By comparing the SolidWorks models to the alternator simulations, we could effectively improve the design throughout the development of the generator device. To ensure the success of the Gorlov turbine blade design, a fluid-flow analysis was done for the selected

hydrofoil profile. Figure 2 shows a graph of the lift coefficient versus the drag coefficient for the optimized hydrofoil (green) and a standard NACA0012 profile. The results of the team's simulations helped to confirm the design and allowed for the manufacturing to begin.

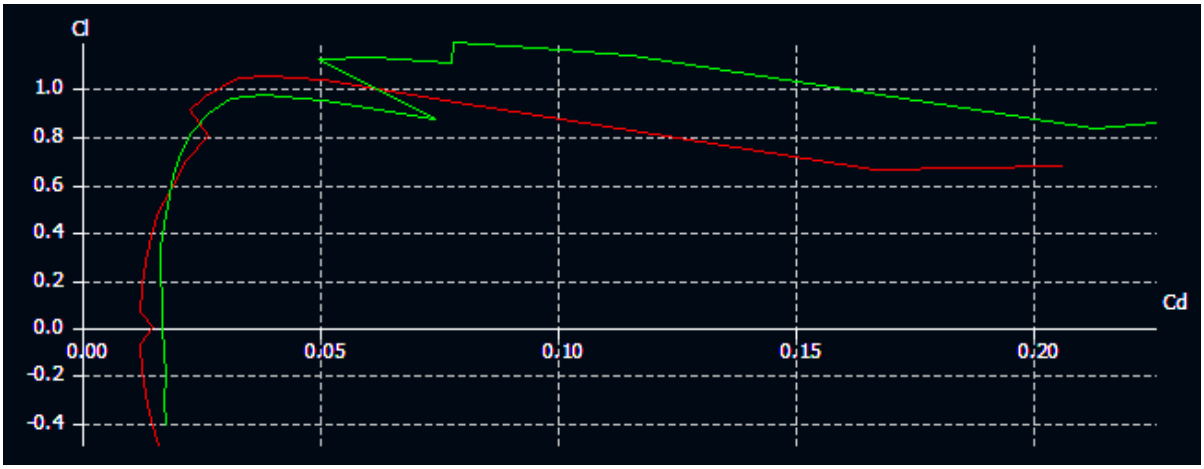

Figure 2: Simulated Profile in Comparison with NACA0012

Using MakerBot Replicator 2 Rapid Prototypers, the helical blades for the turbines were created. For ease of manufacture, the blades were manufactured in halves and later assembled together. In addition to the helical blades, several frame and alternator pieces required CNC machining. Through the development of Esprit CAM files and the use of a HAAS, VF4 Mill and CNC Lathes the alternator casing, frame cross members, axle, alternator core spacer and alternator core were developed. Finally, the team made use of a Universal Laser Systems laser-cutter printer to create a mold for magnet placement, acrylic spacers for coil development, and the triple arm blade plates. After the appropriate pieces had been made, the device was assembled and sealed using silicon caulking. The final alternator design features two diametric flow helical turbine blade sets with one alternator center mounted between them. Each turbine featured three blades rapid prototyped to an optimized hydrofoil profile. The turbines directly drive a coreless-stator, synchronous, three-phase alternator consisting of two, sixteen-magnet rotors sandwiching a twelve-coil stator. The entire design was developed to be watertight for functionality in any submerged environment. The final device and all prior iterations are described at length later in the report.

After the device was manufactured and assembled, it needed to be tested accordingly. First, dry tests of the alternator were conducted in WPI's Atwater Kent labs. Tests were executed to determine the stator resistance

as well as the induced voltages, currents, and power outputs of the alternator at a various rotation speeds. These tests showed the three-phase power output to be sinusoidal and well-balanced.

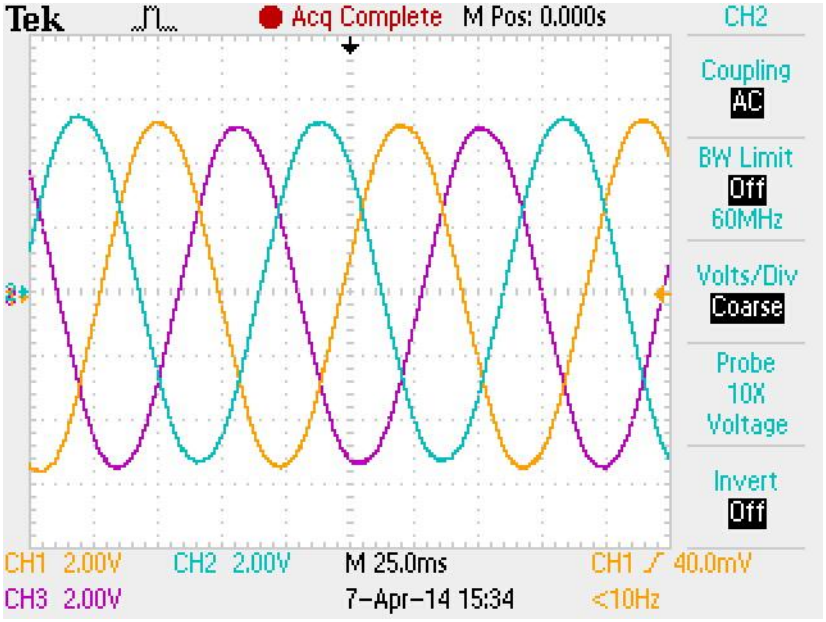

Figure 3: Three-Phase AC Voltage Waveform from Dry Testing

The voltage waveform in Figure 3 above was produced during the dry testing. In order to produce an environment similar to a steady liquid current, the device was tested using the WPI Recreation Center's adjustable flume speed rowing tanks. The device was fixed into the tank via fabricated legs and ropes. The tests included running the machine in water at speeds up to 6ft/s (1.8m/s) to record the resulting machine revolution speed, output power, voltage, and current.

The flume speeds used, resulted in the turbine rotating at speeds between 45 RPM and 180 RPM. These tests were repeated with 20Ω and 5Ω loads, per phase. The device was also tested on the lowest available load, 3.7Ω, at the highest flume speed, 6ft/s (1.8m/s) to obtain a "maximum" power output for the experiment. The maximum output was measured at 9.5W for one of the three AC phases, so total output power was estimated to be around 28-30W.

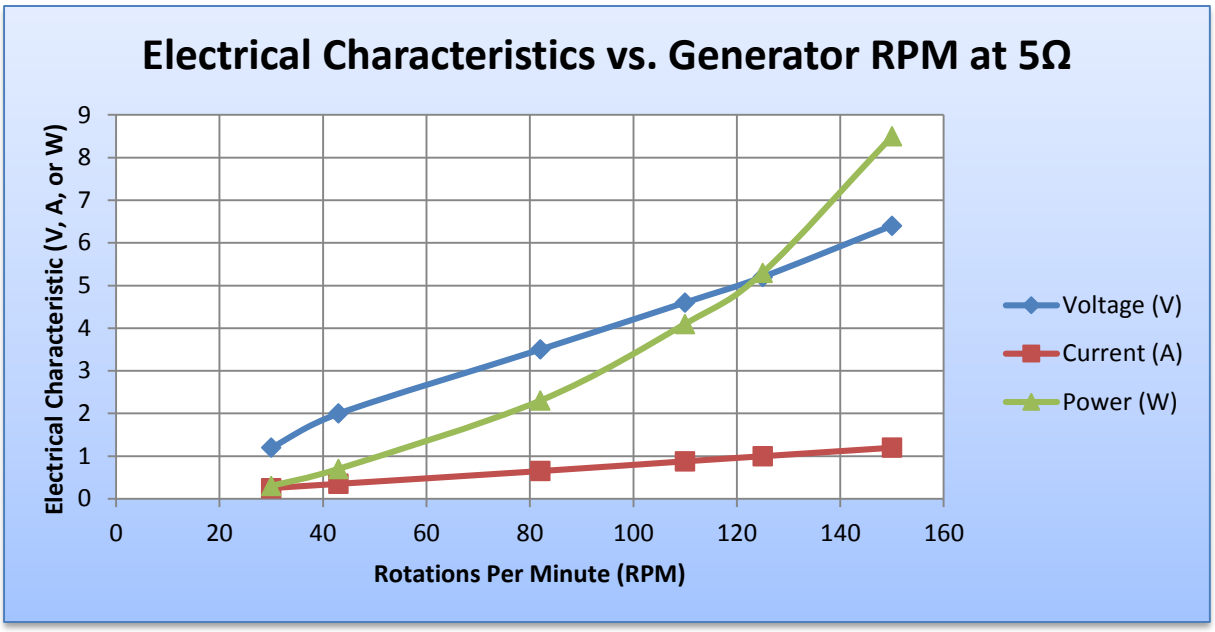

Figure 4: Power, Voltage, and Amperage vs. RPM for 5Ω trials.

Figure 4 above shows the power, current and voltage versus rotations per minute for the device when connected to the 5Ω resistors. When the turbine is spinning at around 125 RPM, power begins to increase exponentially as voltage and current increase linearly. Since the device is scalable in size, a larger device designed for high RPMs could generate significantly more power than voltage and current, which can be controlled through specialized electronic circuits.

Once this information was collected and compiled, it was analyzed by the group. Based on the information that was obtained, conclusions, recommendations and analysis of device performance were made and are included in the report. The power that was created is enough to charge a small battery but did not achieve the full output power that the project team was hoping to create. The device was able to accept a linear liquid current-based input and produce a three-phase AC power output, with very little visible cavitation across the turbines. Despite not achieving the desired output power, the device was still a successful proof-of-concept prototype, and with improved manufacturing accuracy, the output power would increase. Future research could focus on minimizing the air gap, maximizing the coil turns, analyzing the effects of a cored stator, or even constructing larger models to test scalability.

TABLE OF CONTENTS

TABLE OF FIGURES

TABLE OF TABLES

INTRODUCTION

MOTIVATION

In 2003, Nobel Laureate Richard Smalley presented the “Top Ten Problems of Humanity for Next 50 Years” which identified energy as the number one problem. Smalley explained that all of the remaining problems facing humanity could be solved if the energy problem was solved. Oil and other fossil fuels currently supply most of the energy that is consumed by humans, but these fuels will eventually run out and the byproducts many of these fuels harm the planet. The global focus on clean and renewable energy sources, such as solar, hydro and wind power, has increased dramatically in the past few decades and continues to do so. As prospective engineers, we had the technological know-how and the passion to develop a device capable of producing clean, electrical power. This project sought to develop a small-scale, scalable, hydropower generator device as a proof-of-concept prototype.

AVAILABLE OCEAN POWER

In the modern age, there is high demand for a consistent and efficient source of renewable energy. As the prices of oil and fossil fuels rise and supplies diminish, interest in renewable energy is on the rise (Air Fuel Synthesis, 2014). Ocean power is not a new concept, but prototypes and major developments in the field have only been around since the late 80's to early 90's. As a result, very few systems are integrated with the electrical grid and have yet to see real practical use. However, new technologies are starting to open the potential for ocean power in a variety of different applications.

Since about three quarters of the Earth’s surface is covered in water, there exists a vast network of untapped energy in the form of wave, tidal, underwater (marine) currents, and even thermal systems.

Form of Ocean Energy	Estimated Global Resource (TWh/yr)
Tides	300+
Waves	80,000
Tidal (marine) current	800+
Thermal gradient	10,000

Figure 5: Estimated Ocean Power Resources (Burman, Kari, Walker, 2009).

Pictured above in Figure 5 are the estimated global resources for each of the main ocean energy sources. Most of the energy in the ocean can be found in the form of waves, at approximately 80,000 Terawatt hours per year (TWh/yr). In the U.S alone, tidal current and wave potential could provide about 400TWh/year, or 10% of the current annual national energy demand (Burman, Kari, & Walker, 2009). While plentiful in resources, both tidal and wave energy has its shortcomings compared to other major renewable sources. Location plays an important role, because while tidal and wave patterns are consistent in localized areas, they vary all over the world. While it is too early to adequately assess environmental concerns, new prototypes for large scale deployments require federal approval, especially when connecting to the electric grid. Despite these limitations, the abundant energy supply of the ocean combined with recent technological developments has huge potential for the future of ocean power applications. The biggest challenge will be able to identify the most cost effective, efficient, and reliable method of converting mechanical energy to electrical energy.

WAVE POWER

Waves are created by the movement of the atmospheric fluids (due to solar heating of the Earth) against the movement of the ocean below its surface making a volatile surface texture, ocean waves. Most wave power devices use the change in kinetic energy (the bobbing motion) in the waves to pump fluid into turbines in order to create electricity. The amount of power generated by the device is dependent on the frequency and amplitude of the waves. At latitudes closer to the Earth's poles, wave energy levels can be up to ten times higher than around the earth's axis (Burman, Kari, & Walker, 2009).

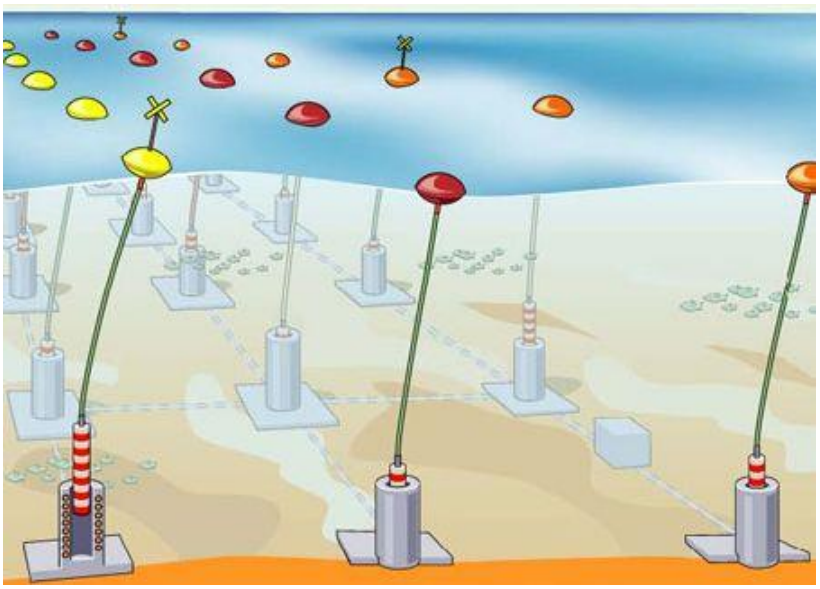

Figure 6: Wave Energy Converter Concept (Streeter, 2008).

Figure 6 above depicts a modular array of buoys that sway with the movement of the waves. Two of these buoys, which are installed off the coast of an island in western Sweden, provide enough energy for 20 households. Typically, each buoy device acts independently of one another and contains a generator. These units can then be connected together so that the power is essentially proportional to the number of units, as shown above.

TIDAL POWER

Tides (although often confused for waves), are caused by the moon's gravitational pull approximately every 12 hours rather than the ocean surface conditions. Devices use the potential difference in water height from low tide to high tide to produce electricity, which can amount to 1000MW of instantaneous power in some locations. In order to be capture enough power, the difference between the tide heights must be at least 16ft. Unfortunately, only 20 to 40 locations on Earth consistently have this capability, thus severely reducing potential use (Burman, Kari, & Walker, 2009). Also, it is not realistic to form a small-scale tidal power device since it is typically a barrage or dam that requires placement in a large waterway.

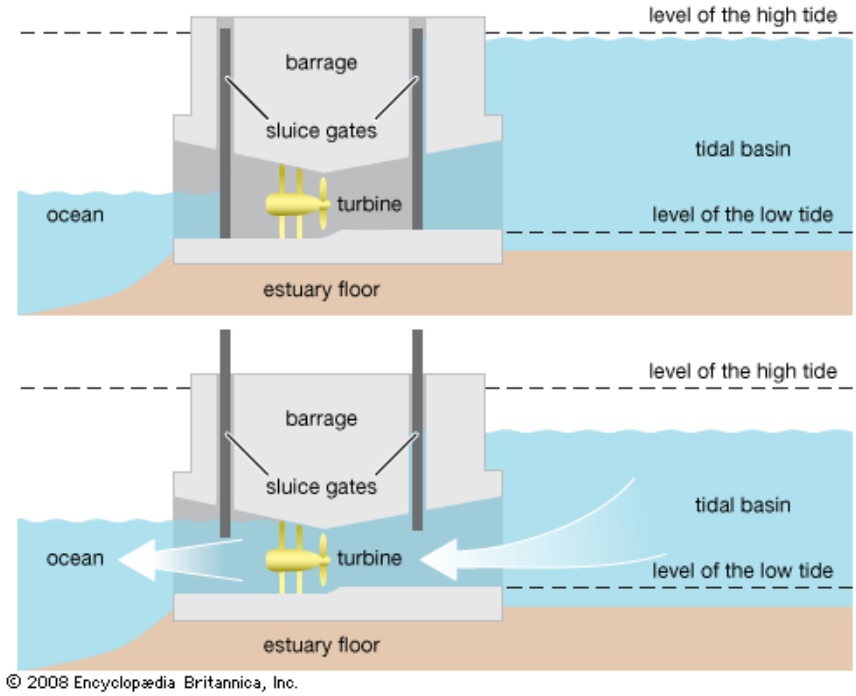

Figure 7: Tidal Power Generation Concept (Lehigh University, 2010).

Most tidal power generators are very large barrages that must be capable of capturing the energy from masses of water moving in and out. Although tidal power has an estimated resource of 10,000TWh/yr, it can be very costly and difficult to deploy an effective prototype. As depicted above in Figure 7, sluice gates which control the flow of water through the turbine are closed at high tide. During low tide, when the height difference is greatest between both sides, the sluice gates are opened and a massive surge of water is sent through the turbine.

CURRENT POWER

Devices that harness power utilizing water currents appear commonly in industry, where bulk fluid flow is more predictable and stable. Marine currents are bidirectional and reverse once every six hours on average.

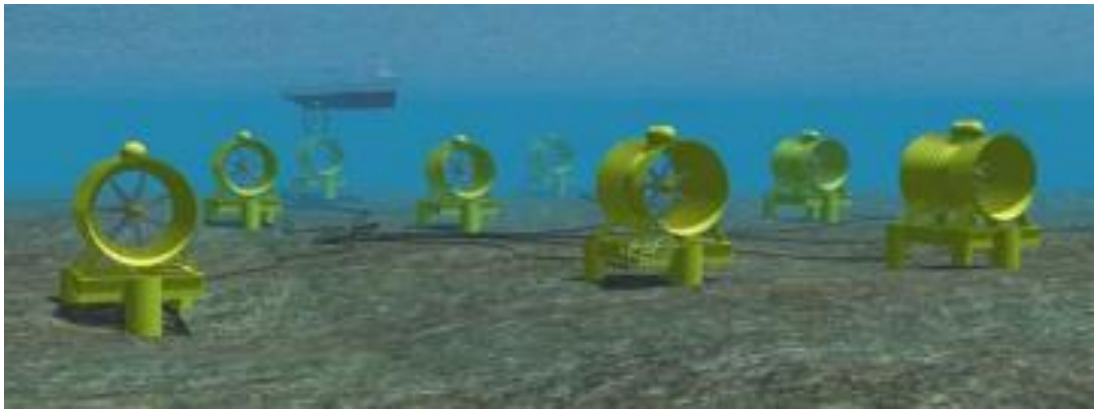

Figure 8: Rotech Tidal Turbine (Burman, Kari, Walker, 2009).

Sea water is 800 times denser than air, so turbines for marine current applications can be smaller and more compact. This also means that the power in a 12mph current is the same as a 110mph gust of wind. Shown above in Figure 8, is an array of underwater turbines (analogous to a wind turbine farm) placed in underwater conditions where tidal/marine currents are strong enough. The blades are also shaped to account for the bidirectional flow of the water. With an estimated 5000GW of total current energy found throughout the globe, harnessing water current is the most common application of ocean power (Burman, Kari, & Walker, 2009).

ALTERNATOR TOPOLOGIES

In order to select the appropriate alternator configuration for the underwater generator device, it was necessary to observe advantages and limitations of commonly used topologies. Two specific types, radial and axial flux alternators, where analyzed in terms of power output, alternator efficiency, ease of construction, and device application.

RADIAL FLUX

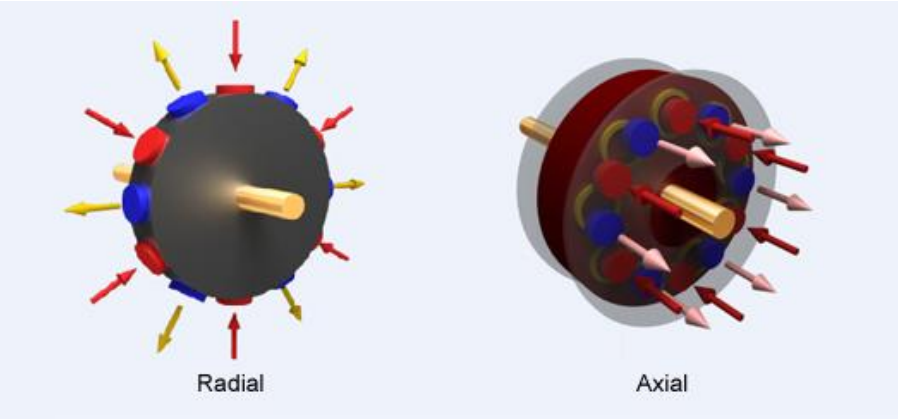

Figure 9: Radial and Axial Flux Topologies with Flux Propagation (Microsun - Free Energy, 2013).

In a radial flux alternator, magnetic flux propagates perpendicular to the axis of rotation. Figure 9 above shows how the flux is bidirectional in both cases, but either perpendicular or parallel to the shaft. Most radial flux alternators have a very low diameter to length ratio, thus the flux is “bottle-necked” and flows in a radial direction. However, this means there is poor heat dissipation inside the alternator (Gieras, Wang, & Kamper, 2004).

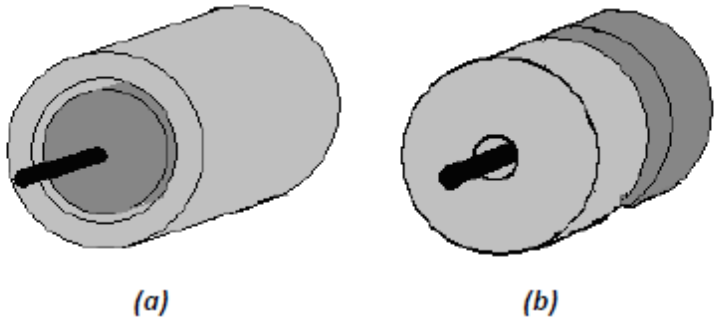

Figure 10: Radial Flux Alternator Construction (a), Axial Flux Construction (b) (Strous, 2010).

Proper construction tends to be more costly and challenging compared to axial flux machines, in which the rotors can be easily equipped with electric steel. There are also large attractive forces between the stator and rotor that requires assembly to be precise, thus further increasing manufacturing costs. Figure 10a shows the rotor (dark gray) on the axis of rotation enclosed within the stator (light gray), while Figure 10b depicts the rotor (dark gray) and stator (light gray) "stacked" through the center axis.

AXIAL FLUX

In an axial flux alternator, the magnetic flux is propagated parallel to the axis of rotation. Since the stator is "sandwiched" in between a double rotor, it uses much less winding per coil than a radial flux alternator. Overall, these alternators have a larger diameter to length ration meaning better cooling and ventilation. This topology can also accommodate more magnetic poles because the air gap (distance between the magnets) can be easily adjusted. In addition, axial flux machines can generate more torque than the radial flux machine with similar outer radii. Typically, axial flux alternators weigh less overall and would be more suitable for underwater applications (Colton, Mularcik, Kennedy, Camilleri, & Rohoza, 2009).

A university in Finland tested both alternator topologies for small-scale wind power production in order to determine the optimal configuration. They found that by applying the same force of wind to both alternators (keeping the same rotational speed and torque values), there was a notable increase in efficiency with the axial flux alternator at lower speeds than radial flux:

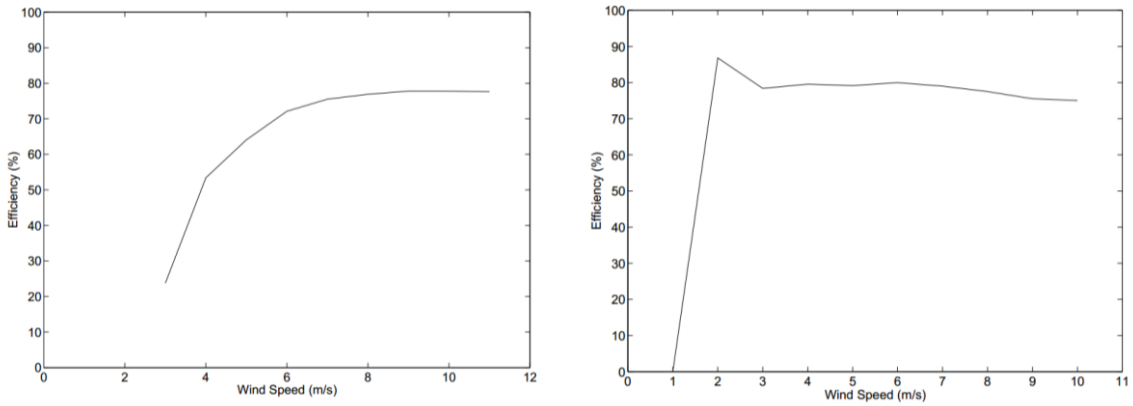

Figure 11: Efficiency vs. Wind Speed of Radial Flux (left) and Axial Flux (right) (Rovio, Vihriala, Soderlund, & Kriikka, 2014)

While Figure 11 depicts efficiency results for wind applications rather than water currents, it stands to reason that radial flux alternators perform poorly at low speeds and not notably any better at higher speeds, than its axial flux counterpart. For this project, it makes more sense to use an axial flux topology since low speeds and high efficiency are important to optimize power output.

TYPES OF TURBINE SYSTEMS

There are a large variety of turbines that the group investigated for applications in this project. The group began by looking into the various types of turbines commonly used in wind and water conversion. We discovered that there were a limited number of turbines commonly used for natural electromechanical energy conversion. These turbines can be separated into two groups: Horizontal Axis Turbines, and Vertical Axis Turbines.

HORIZONTAL AXIS TURBINES

Horizontal Axis Turbines (HATs) are turbines which rotate along an axis parallel to the fluid flow. Traditional wind turbines are a great example of this type of system. This type of turbine uses the bulk flow of a fluid, either air or water, to rotate a set of blades. The blades typically need to be orientated in the direction of flow to maximize their efficiency (Niblick, 2012).

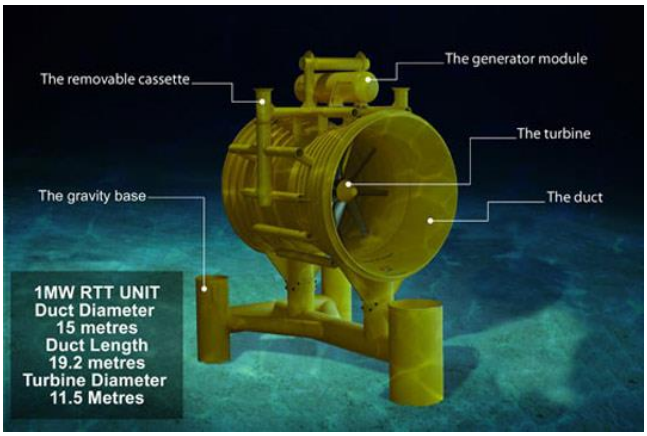

Figure 12: A Horizontal Axis Water Turbine (Basantani, 2008)

While the majority of HATs are used in wind applications, there are also applications of HATs in hydropower applications. Figure 12 shows an example of a possible horizontal axis turbine for underwater use. However most systems taking advantage of this concept do not use passive liquid flows. Typically HATs underwater use a forced flow to maximize rotational force, as can be seen in any hydroelectric dams or forced internal pipe applications.

VERTICAL AXIS TURBINES

Vertical Axis Turbines (VATs), contrary to HATs, operate with their axis of rotation perpendicular to the fluid flow. These turbines have several advantages and disadvantages compared to HATs. VATs can be used for omnidirectional flow without requiring any change in orientation for varying flow direction. They also have comparably lower tip speeds and operate much quieter than HATs due to the fact that they capture passive resultant fluid flows. VATs, however, have not been utilized in as many power generation applications as HATs. Additionally, there are several different types of VATs each with its own benefits and detriments depending on the application environment.

SAVONIUS TURBINE

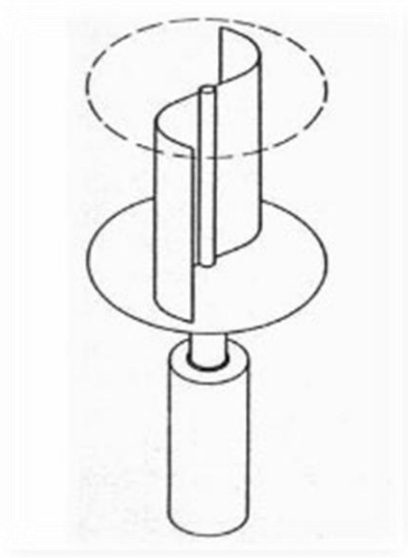

Figure 13: A Savonius Type Vertical Axis Turbine (Savonius Wind Turbines, 2014)

The Savonius turbine is a simple, effective type of VAT. Savonius turbines are drag based turbines, meaning they utilize fluid drag as the driving force for the turbine. The Savonius turbine uses an S shape in order to catch the fluid flow and spin the turbine. The scoop shape of the blades creates less drag on the return motion than the driving motion, allowing the turbine to spin. Figure 13 shows the shape of a Savonius turbine.

Savonius turbines are advantageous in that they are very easily built, as the blades are simply half cylinders or a comparable concave shape. They operate very well at low speeds, and can produce high torque as compared to other turbine blade options. Savonius turbines are fairly inefficient though, as drag-type devices are unable to accelerate beyond the speed of the fluid and are fairly difficult to integrate into use with an alternator (Niblick, 2012).

DARRIEUS TURBINES

Another type of VAT that is commonly used is the Darrieus turbine. In contrast to a Savonius type, the Darrieus turbine is a lift based turbine. Instead of using drag to "push" the turbine blades, it uses an airfoil profile to create lift as a driving force. Figure 14 shows a typical type of Darrieus turbine for wind applications.

Figure 14: A Darrieus Vertical Axis Turbine (Aarchiba, 2007)

The H-Darrieus turbine, a slightly modified version of the Darrieus turbine, uses straight blades instead of curved blades, and commonly employs three or four blades as opposed to just two. An example of an H-Darrieus turbine can be seen in Figure 15 (Niblick, 2012).

Darrieus turbines are very advantageous for use with alternators as the airfoil blade shape produces a very high tip speed. Additionally, H-Darrieus turbine rotors are easy to manufacture aiding in their accessibility, a key characteristic for energy conversion devices. Darrieus turbines have a significant drawback in that they are unable to self-start. The turbine is unable to produce enough force in order to start its motion from a stopped position (Gorlov, 1998). This requires the introduction of a small starting force. Despite this flaw, Darrieus turbines are used, with some modification, in wind applications as well as some use for hydroelectric applications.

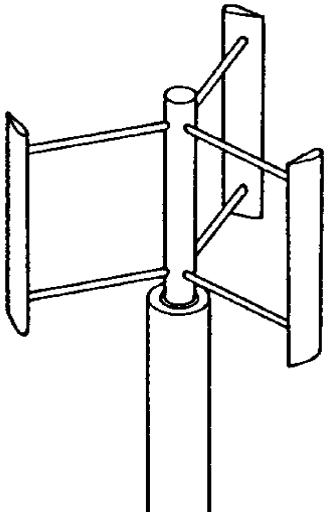

Figure 15: An H-Darrieus Turbine Configuration (H-Type Darrieus Turbine)

HELICAL TURBINES

Another type of VAT is the helical turbine. Helical turbines, first developed by Northeastern Universities' Alexander Gorlov in the late 90s, have seen recent public interest. An example of a helical turbine can be seen below in Figure 16:

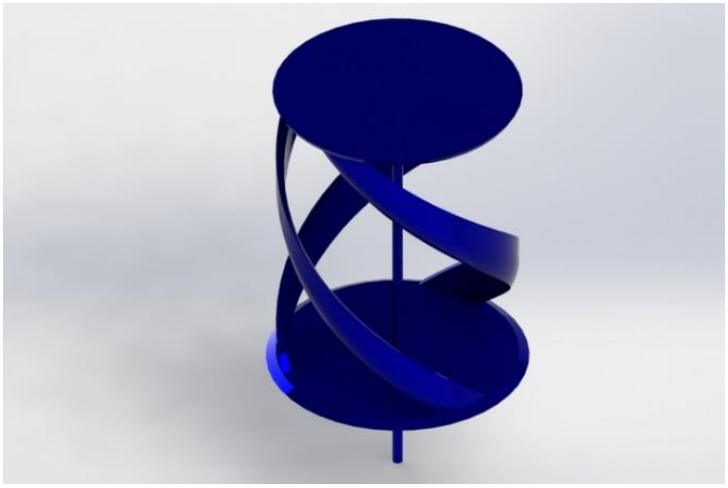

Figure 16: A Helical Turbine (Helical Turbine, n.d.)

Helical turbines, like Darrieus turbines, use an airfoil shaped blade. This blade profile is used to create lift from the fluid flow moving over its surface. Unlike a Darrieus turbine, the airfoil profile of the blade is twisted along a helical path following the circumference of turbines rotation. This twist provides a consistent blade surface area perpendicular to flow regardless of changing rotation angle, thereby minimizing the losses due a changing angle of attack in each individual blade. A helical turbine also improves upon the Darrieus turbines self-start flaw as the constant flow perpendicular surface area providing constant lift also acts as an optimal lift point on an immobile blade inherently inducing rotation (Niblick, 2012).

THREE PHASE, AC TO DC, BOOST CONVERTER

In order to properly utilize voltage generated from three out-of-phase AC sources, it is necessary to implement a bridge rectifier circuit. An AC-DC converter is not a complicated circuit, but is necessary to reduce electric losses by raising the output voltage while lowering the current. Each of the three phases from the alternator is represented as three independent voltage sources connected to an array of six diodes. This diode array is responsible for capturing only the peak amplitudes of the three signals while they cycle through rapidly. It is then necessary to pass the rectified DC voltage through a "boost" converter, or step-up converter, to amplify incoming DC voltage to approximately 28V. The result is a clean DC waveform with an output voltage that triples the input voltage per phase. Below is a circuit schematic made in ADS (Advanced Design System):

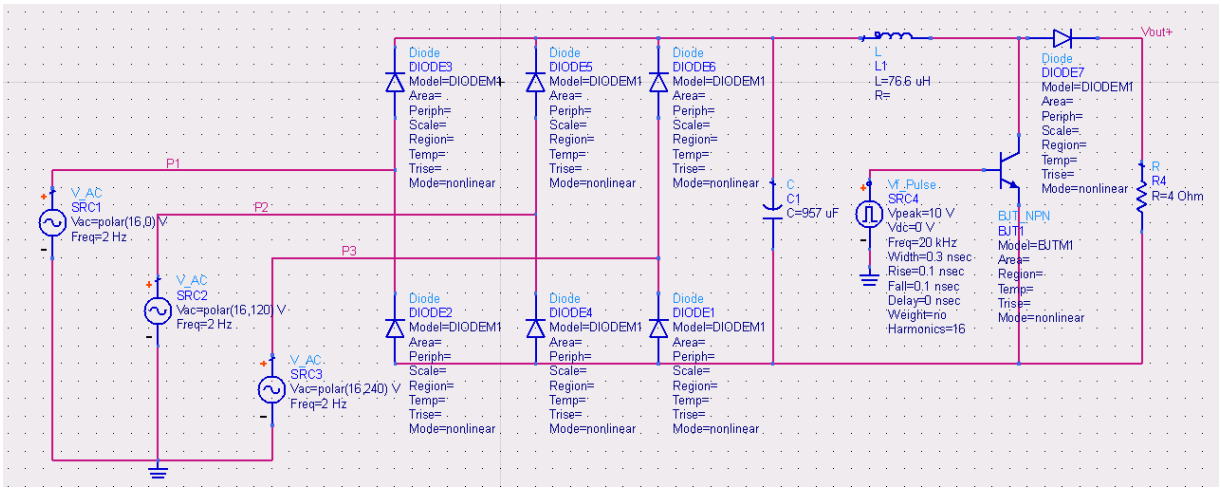

Figure 17: Three-Phase AC-DC Converter with DC Boost Converter

The circuit above in Figure 17 represents a full wave bridge rectifier without a center-tapped transformer. While not essential, placing a transformer before the diode array that can split the voltage evenly across the output allowing for more control and improved harmonic performance (Linear Power Supply & Heat Sinks, 2007).

In comparison, a three phase half wave circuit uses three diodes instead of six, one connected to each power supply. This rectifier mode was not chosen because of its inability to produce a clean DC output signal without harmonic distortion. In the design above, six diodes where used modeled with basic parameters for a Motorola high voltage Schottky diode. Standard diodes typically have a forward voltage drop of 0.7V, while

Schottky diodes only have a drop of 0.3V and are designed for high speed switching applications. Loses in rectification circuits less than 12V are particularly crucial, so selection of diodes does impact design performance. Thyristors are more suitable for HVDC (high voltage direct current) applications and can be used as a replacement for the diodes since they behave exclusively as bi-stable switches, but are not essential for charging a portable battery (Sastry, 2005). For applications requiring electrical grid connectivity, it may be more suitable to use thyristors.

Each of the three voltage sources is estimated to give approximately 8.8V peak to peak, which is equivalent to the per phase voltage. For rectification to work, the sources must be 120° out of phase and will require three independent function generators to power. Together, the three phase input voltage signals and corresponding DC output given from the rectifier looks like the following:

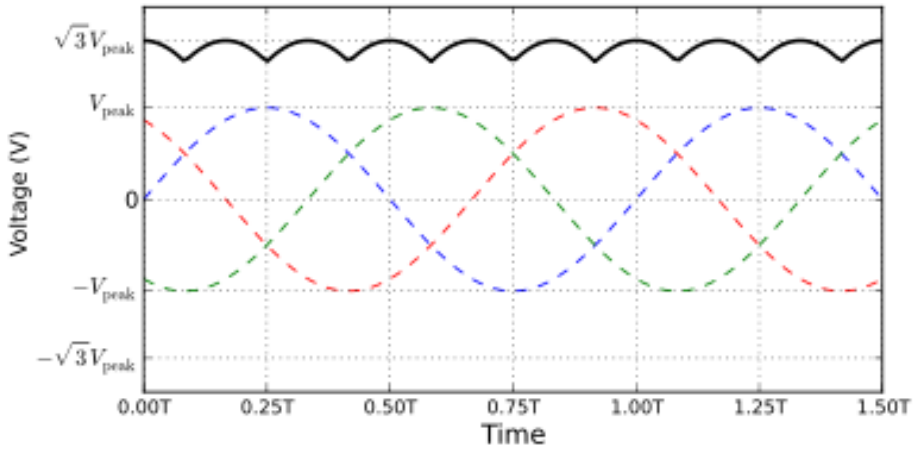

Figure 18: Full Wave Rectifier with Input AC voltage Sources and DC Ripple vs. Time

In the plot above, the top black line represents the DC output (with minor ripples) as a sum of all three input waveform peaks. The ripple voltage is a result of the rectifier's inability to convert all incoming AC voltage to DC, so some unwanted "residue voltage" still makes its way to the output. However, having a larger capacitor (in the range of 100µF to 1mF) after the diode network decreases the voltage ripple significantly.

Modeling the boost converter segment requires integration of a PWM (pulse width modulation) device to drive a semiconductor switch. A pulse voltage source operated at a specific switching frequency (f_s > 20kHz) and low voltage (V_p < 5V) can connect to the gate pin of a semiconductor switch, which could be either a MOSFET or BJT (Bipolar Junction Transistor).

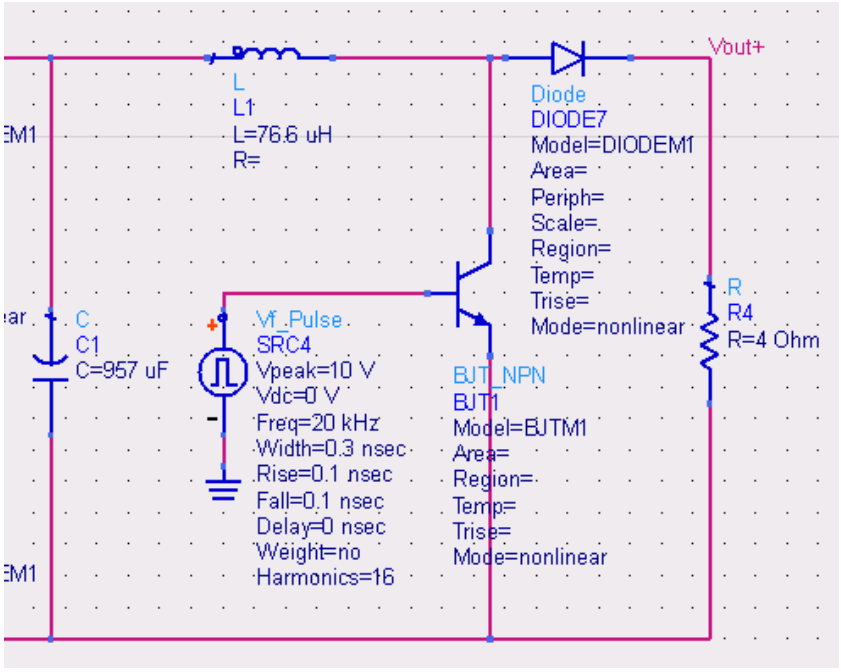

Figure 19: The Boost Converter Circuit, Magnified to Show Parameters

The inductor value for the boost converter was selected to be approximately 75µH, which is reasonable for a low power output design. Capacitance was approximated to be 1mF since the load current is relatively high (I=5.8A) compared to the estimated output voltage of 28V. The load resistor, modeling a 12V battery, can have an internal resistance anywhere between 0.4Ω to 4Ω, but depends on the manufacturer and condition of the battery (Teslaco.com, 2011).

PRIOR ART AND EXISTING SYSTEMS

While engaging in background research, the group found a wide variety of micro-hydropower products leading to the design choices and specifications of this project. The only in use helical turbines were country funded infrastructure projects on the scale of hydroelectric dams. In 2002 the Korean Ocean Research and Development Institute began testing of a 15ft helical turbine in the 12kn current between the Korean peninsula and Jindo Island. In 2012 the Ocean Renewable Power Company (ORPC) began testing the first US permanent installation of a large scale helical turbine. Both projects have been mostly successful and have led to further developments and planned future installations. Our project maintains its individuality in its micro power modular application.

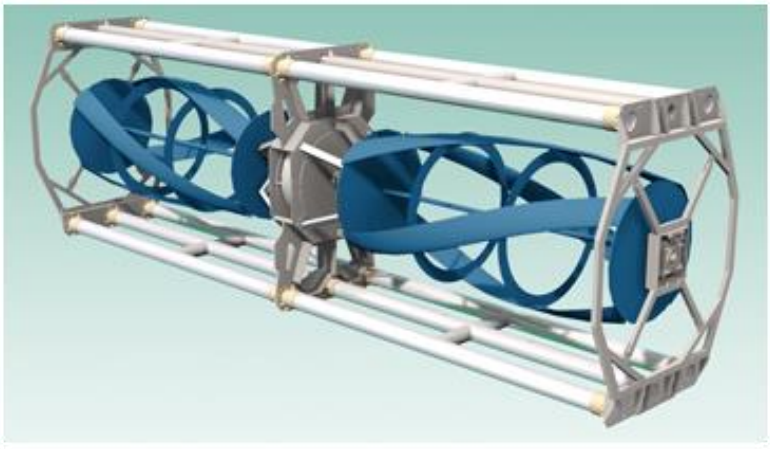

Figure 20: Ocean Renewable Turbine Generator Unit (Cobscook Bay Tidal Energy Project, 2012)

The team's current design iteration bears many similarities to the overall shape and composition of a TGU developed by ORPC pictured above. This design implements two helical turbines directly driving the permanent magnet alternator framed directly in the center. To maximize effectiveness at ocean sites, ORPC usually installs multiple TGUs at once and adjusts them based on location to maximize power for grid connection. The versatility, portability, and lightweight design of this TGU influenced the group's product specifications.

Figure 21: Ocean Renewable Power Company's Large Scale Marine Current Generator (Cobscook Bay Tidal Energy Project, 2012)

Figure 21 shows the company's most recent development designed for large scale applications. This product was released officially to the public while the MQP was already underway. Again, the prototype exemplifies the growing popularity of helical turbines directly driving a permanent magnet, axial flux alternator. In theory, almost every aspect of the team's generator, including the blades, alternator and housing, could be scaled to a larger size for greater power gain.

GENERATOR DESIGN

The following section details the methods the project team utilized in order to design, manufacture and test the prototype. It will highlight the key aspects in each step of the process and provide a summation of the work completed. After the team had amassed an operating knowledge through background research, the next step was to initiate the design. In order to begin the process, the group generated a collection of design specifications for the machine.

DESIGN SPECIFICATIONS

To begin the project team created specifications to restrain the design. These specifications pertained to three main categories; size, materials and functionality. In addition to these the team recognized that the device produced for the project was to be a proof of concept machine; for real world installations further considerations, beyond the MQP scope, would need to be made. All design specifications can be found below:

Materials

- The device must be capable of being built for under $700
- Materials must be easy to manufacture with WPI equipment and at team member's homes
- All electrical components must be watertight

Functionality

- The device must be capable of outputting at least 100W of power
- The device must use a permanent magnet alternator
- The machine design should feature system modularity, allowing two devices to be easily linked together to compound performance in larger application areas
- The device must run continuously; requiring no external reset, start or stop
- The device must be able to self-start
- The device must be capable of running underwater
- The device must passively utilize the motion of ocean currents

- The device should be able to accept input flow from various orientations

Generator Size

- The device must be smaller than 12in x 12in x 3ft (.3m x .3m x .9m) to fit within the testing location
- The device must weigh less than 100lbf

Real World Considerations

- All external materials need to be able to resist corrosion due to salt water
- The device must be able to withstand submersion pressures
- The device must be designed so that it can survive storm conditions
- The device must be outfitted with entanglement barriers without restricting current flow
- An electrical link system must be developed to send power from the device to the shoreline

SYMETRICAL DESIGN INTENT

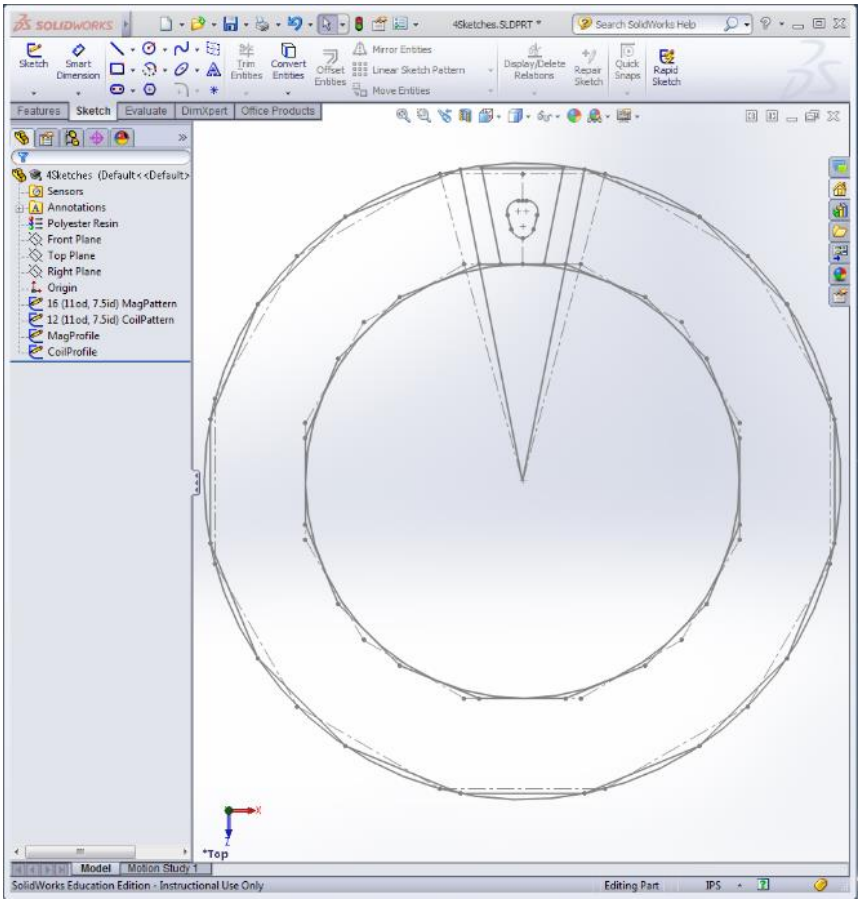

Figure 22: Universal Alternator Dimensions Sketch

The 3D design model needed to be easily adapted to reshaping, resizing, and part replacement as research continued and assumptions improved. This posed a challenge in 3D component modeling. Using Dassault Systems SolidWorks, program base sketches were created to build components off of. This allowed for the limiting machine dimensions to be adjusted at the most basic sketch level of each part. In addition to this, model parts maintained the fewest number of features possible and were then combined into assemblies simulating production procedures and possible assembly methods. The final machine consisted of three main components built off Figure 22's four sketches; the alternator, the turbine blades, and the frame.

ALTERNATOR DESIGN

In order to convert the rotational energy of the turbines into electrical energy, an alternator was used. Of the two major types of alternators, radial and axial flux, the axial flux typology has a higher diameter to length ratio. For the purpose of maximizing the cross sectional area of the turbine, relative to the overall device size, an axial flux configuration was thus selected. An axial flux alternator can be designed in a variety of ways. Other than induction machines, axial flux alternators can be DC commutators or synchronous machines. The machine can be designed with or without a core and or armature slots, with internal or external permanent magnets, surface or interior permanent magnets, and or single or double sided. If a double sided design is chosen, either external rotor or external stator configurations may be adopted (Gieras, Wang, & Kamper, 2004).

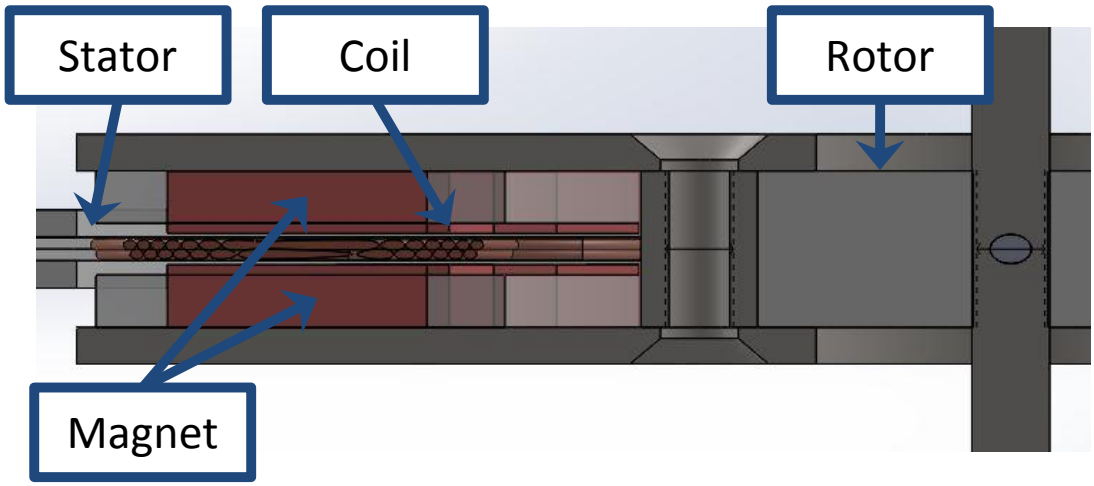

Figure 23: Axial Flux Alternator Configuration

For the design of the alternator, pre-existing designs and concepts were analyzed and chosen from. For the alternator topology, a double sided configuration was chosen, utilizing an external rotor, slot-less armature that "sandwiches" an internal coreless stator. The magnets on the rotor are surface mounted to inner faces of the rotor plates, just off the surface of the suspended stator. Figure 23, above, shows a cross sectional view of the alternator. This configuration is advantageous for slot-less configurations due to good utilization of the stator windings and the high flux density in the windings (Caricchi, Crescimbini, Fedeli, & Noia, 1994). When deciding between designs, the following factors were taken into account: Cost, weight, manufacturability, alternator performance.

Table 1: Design Matrix for Axial Flux Alternator

	Cost	Weight	Manufacturability	Alternator Performance	Total
Weight of Factors	**3**	**1 (Least Important)**	**2**	**4 (Most Important)**	
Stator Core					
Cored Stator	✗	✗	✗	✓	4
Coreless Stator	✓	✓	✓	✗	6
Rotor Topology					
External Rotor	✗	✗	-	✓	4
Internal Rotor	✓	✓	-	✗	4
Magnet Topology					
Surface Mount	-	✗	✓	✓	6
Embedded Mount	-	✓	✗	✗	1
Rotor Material					
Grain Oriented Silicon Steel	✗	✓	-	✓	5
Low Carbon Steel	✓	✗	-	✗	3
Magnet Material					
Samarium Cobalt	✗	-	-	✗	0
Sintered NdFeB	✓	-	-	✓	7

Table 1, above, shows some major design choices. Designing the alternator to be coreless was a tradeoff that resulted in a cheaper, lighter, and easier to manufacture device, at the expense of alternator performance. A benefit to coreless configurations is the elimination of associated stator core eddy current and hysteresis losses. However, at higher rpm, the slot-less configuration can often have large eddy current losses in the windings. Additionally, all cogging torques are eliminated, resulting in a higher efficiency at lower rpm. Cogging torque is defined as the torque due to the interaction between the permanent magnets of the rotor and the stator coils. This force is undesirable for permanent magnet machines, especially for low-speed devices. Removing this torque force is highly desirable for the alternator configuration. However, adding a core to the stator configuration would reduce the reluctance of the air-gap, thereby increasing the magnetic flux in the circuit. This would in turn lead to higher power production. It was decided that the loss of power production capability of a coreless configuration was acceptable. For the permanent magnet configuration, a surface mount was chosen as this is the typical configuration of a slot-less axial flux topology. (Gieras, Wang, & Kamper, 2004)

ROTOR CORE & MAGNETS

The rotor of the permanent magnet, axial flux alternator consists of the permanent magnets and the rotor core. The original material chosen for the rotor core was 0.025in M36 non-oriented electrical steel as this material is favorable for its magnetic properties. Electrical steel is iron alloy that contains up to up to 6.5% silicon and may contain up to 0.5% aluminum and manganese. By decreasing the resistivity of the steel, silicon causes a reduction in the induced eddy currents and the core losses (Beckley, 1999). Electrical steel components are constructed by stacking laminations of thin, coated steel sheets to make a core. The coating works to reduce eddy currents and increase electrical resistance between laminations. Due to time constraints, the team decided to utilize two 1018 low carbon steel plates purchased from Beaumont Metal Works. This design change decreased the expected performance capabilities of the alternator; however the effect should be minimal. Table 2 shows the resistivity of the silicon electrical steel rotor core and the 1018 steel core.

Table 2: Resistivity of Rotor Steels

Steel Type	Electrical Resistivity (μΩ / cm)
1018 Low Carbon Steel	40 - 50
1.29 M36 ASTM A677 Non-Oriented Steel	15.9

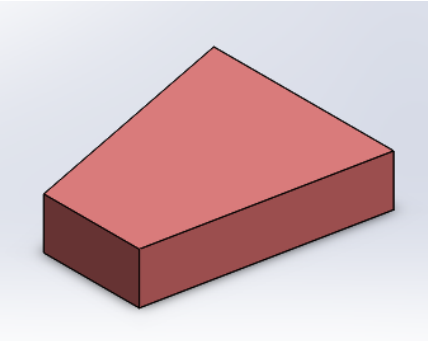

Figure 24: Permanent Magnet Geometry

The permanent magnets, shown in Figure 24 above, are trapezoidal shaped and non-nickel plated. The trapezoidal magnet shape allows for the maximum magnetic material to be attached to the rotor core. By the

suggestion of our supplier, we chose not to nickel-plate the magnets as this will allow for better adhesion between the magnet and the steel core and also reduce degradation of magnet strength associated with the plating process. A benefit to coating magnets is that corrosion resistance is increased, however new techniques in magnetic manufacturing allow for much higher corrosion resistance in un-plated magnets. Samarium cobalt and neodymium magnets were selected as possible permanent magnet materials due to their high remanence and coercivity values. N40 grade, sintered neodymium iron boron was chosen for our design as BJA Magnetics Inc. provided these magnets free of charge. The properties of the magnet material are shown in **Error! Reference source not found.** below (Magnetics):

Table 3: NdFeB Magnet Properties

Magnet Type	Remanent Induction (Br)		Normal Coercivity (HcB)		Maximum Energy Product (BH Max.)	
	Tesla	Tesla	KA/m	KA/m	KJ/m^3	KJ/m^3
	Max.	Min.	Max.	Min.	Max.	Min.
Sintered Neodymium Iron Born N40	1.29	1.26	978	875	318	302
Sintered Samarium Cobalt Magnets YXG-30	1.11	1.08	835	780	240	220

The major benefit of samarium cobalt is that it has a higher tolerance for heat and is less easily demagnetized, as compared to neodymium. Samarium cobalt magnets will lose all magnetic properties at around 800°C while neodymium magnets will lose all magnetic properties at only 320°C (Electronics, 2013). The heat tolerance was not necessary for the expected rpm of our alternator, so the neodymium was sufficient.

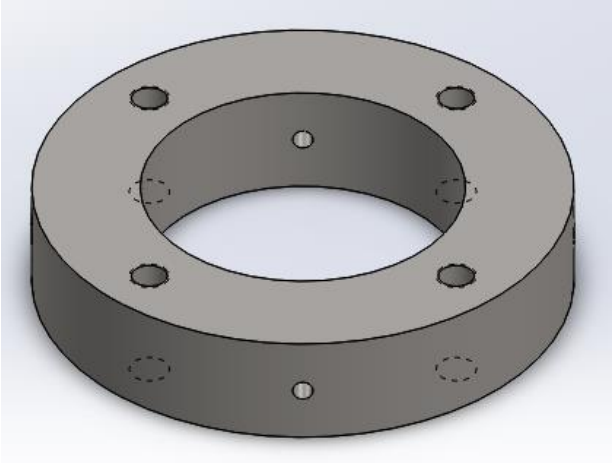

Figure 25: Rotor Core Alignment Spacer

The rotor core is composed of three different parts: two 12in (.3m) diameter washer-like disks (Figure 26) and one thick separator ring (Figure 25) and two rotor plate assemblies. The magnets were attached to the rotor cores via JB Weld and encapsulated in an epoxy resin. Our research indicated that the strength of the bond between magnet and rotor will be sufficient to hold the magnet in place (Chen & Pillay, 2005).

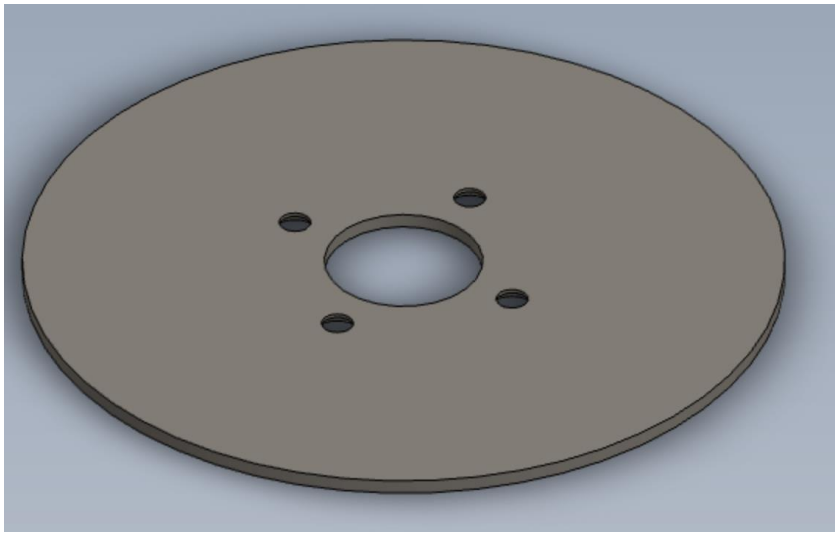

Figure 26: 1018 Low Carbon Steel Rotor Model

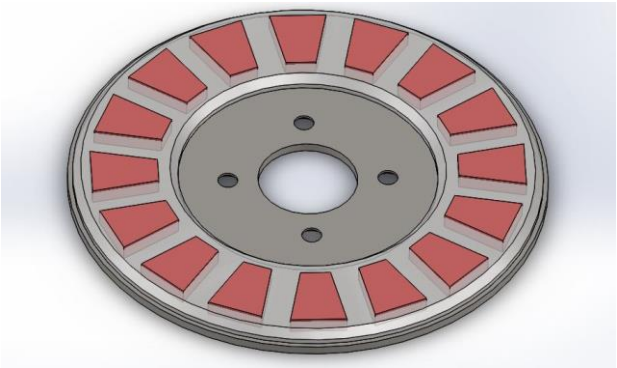

Figure 27: Rotor Core Magnet Plate

For the alternator design, a sixteen magnet orientation was chosen, as shown in Figure 27. For the size of our device and from prior research, we determined this number of magnets to be adequate (Works, 2010). For determining the size of the magnets, we based the trapezoidal geometry on a ratio relating the outer to the inner allowable radii. An optimized design utilized an inner radius to outer radius ratio of 0.68, or R_i / R_o = 0.68 (Wang, Kamper, Van der Westhuizen, & Gieras, 2005). To determine the positioning of the magnets, the centers were then aligned with the centers of the stator coils. The stator coils take up the most possible space within the alternator to maximize the amount of coil turns, so the geometry is set. Figure 28, below, shows the assembled rotor without the top rotor plate.

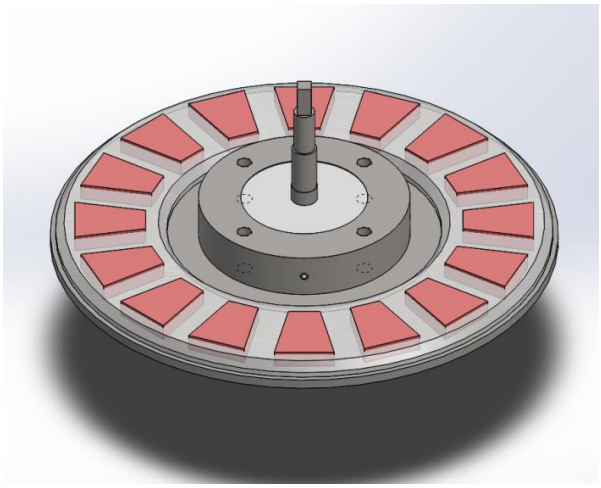

Figure 28: Assembled Rotor with Top Removed

STATOR & WINDINGS

The primary design constraint for the alternator stator was minimizing the overall thickness. As the thickness of the stator increases, the air gap of the alternator increases, resulting in a higher reluctance in the magnetic circuit. This would result in a lower flux density in the air gap, leading to lower power production. The relationship between the air gap thickness and the flux density in the air gap is shown in the Load-Line Analysis section. In order to determine an acceptable air gap for our alternator, we made an assumption about the maximum current the alternator wire would be exposed to (no more than 18A). This allowed us to find a wire gauge that had an adequate ampacity value. Ampacity is defined as the maximum amount of electrical current a conductor can carry before sustaining immediate or progressive deterioration. 16 Gauge wire will have a temperature less than or equal to 90°C if the amperage remains below 18A (Association, 2008).

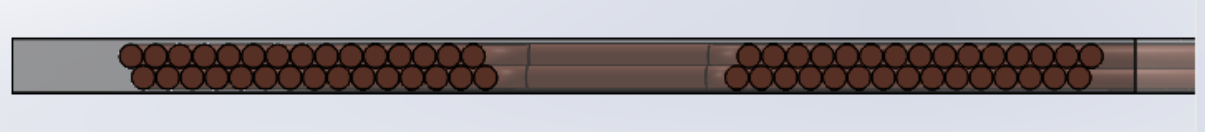

Figure 29: Stator Side Cross-Section

Figure 29, above, shows a side, cross-sectional view of the stator in SolidWorks. There are 30 turns per coil, which was determined based on the maximum amount of turns that would fit with twelve stator coils. It was decided that the stator coils could be no more than three wire diameters tall, for a maximum thickness of 3.873mm per coil, to keep the air gap sufficiently thin.

The SolidWorks model does not show the wiring configuration connecting each of the coils a phase. The series connection of each of the coils in a phase adds an additional wire thickness to what is shown in Figure 29 and Figure 30. Figure 30 shows how the coils in the stator disk could not fit any additional turns or they would overlap, adding thickness.

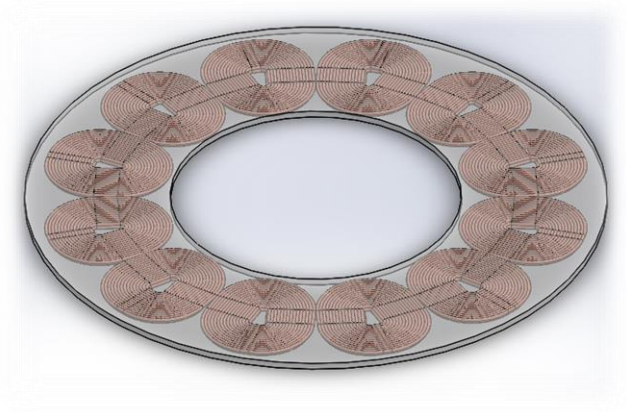

Figure 30: Completed Stator Model

Proper wiring is essential in developing a three-phase alternator. Every fourth coil is connected in series for a total of three phases, each containing four coils. To properly connect each coil, the wire protruding from the center of a coil must connect to the wire protruding from the outer edge of the next coil. One of the ends of each of the three phases are connected to create a virtual ground, while the other end of each phase outputs the power for that phase. Figure 31, below, shows the wiring diagram used while casting the stator.

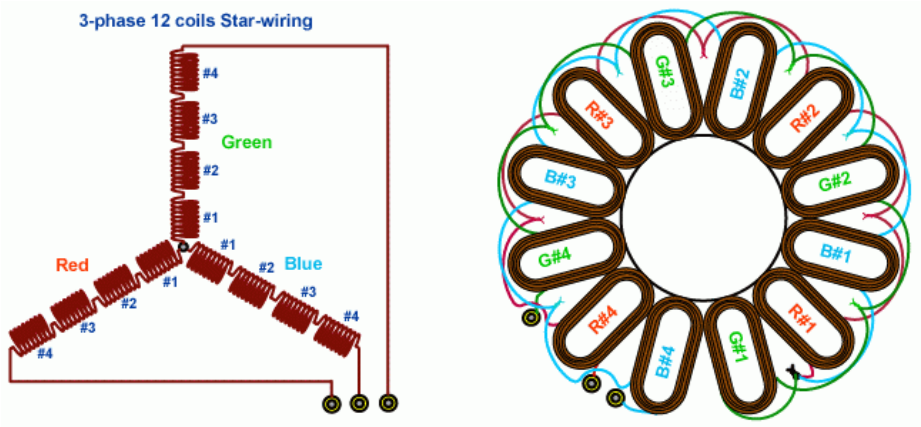

Figure 31: Wiring Diagram for Three-Phase Configuration (Newbie, 2014)

ALTERNATOR 3D MODEL

The model consists of the rotor assembly, the stator assembly, the alternator housing and the axle assembly. Figure 32, below, show an exploded view of the alternator. The alternator is designed to be sealed water tight outside the alternator housing.

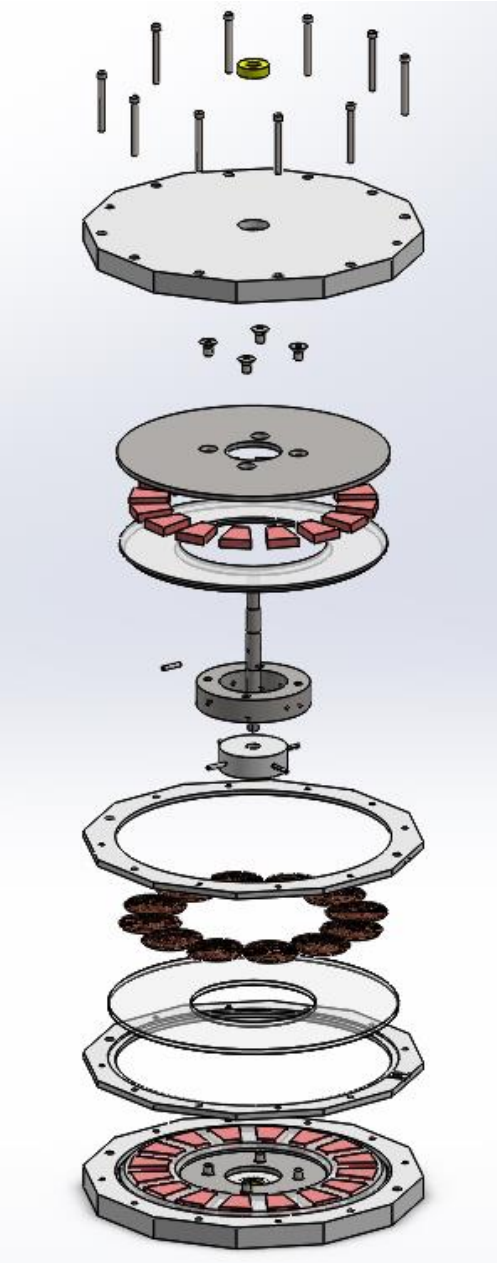

Figure 32: Alternator Exploded View

POWER AND ENERGY

For the purpose of maximizing the cross sectional area of the turbine, relative to the overall device size, an axial flux configuration was selected for the alternator. The thinner alternator allows for the remainder of the device length to be dedicated to the turbines. In evaluating the possible power output of the device, it is important to consider the total power output of free flowing water. Where A_w is the cross sectional area of water flow across turbines, the total power output of free water flow, P_W, is equal to:

$$P_w = ½ \times \rho \times A_W \times v^3$$

Equation 1: Power of a free water current through a cross-flow area

$$P_w = ½ \left(1000 \frac{kg}{m^3}\right) (0.3\, m^2) \left(1.5 \frac{m}{s}\right)^3$$

$$P_w = 225W\ per\ blade$$

$$P_w = 450W$$

The total available water power of 450W is the maximum possible power output of the generator device. However, the output of the device will be much less as we will not reach an efficiency of 100%. The two factors that affect the machine's efficiency are the alternator efficiency and the turbine efficiency. In a non-constrained configuration, the Gorlov helical turbine has exhibited efficiencies of around 35% (Gorban', Gorlov, & Silantyev, 2001). As for the efficiency of the axial flux alternator, modern motors and generators typically run at 90% efficiency and above (Saslow, 2002). Using 35% for the turbine efficiency and 90% for the alternator efficiency, a power coefficient, ŋ, of 0.315 is attained by multiplying the two efficiencies together. By taking this power coefficient into account, an estimate for the total power, P_t, for the device can be attained as follows:

$$P_t = ½ \times ŋ \times \rho \times A_W \times v^3$$

Equation 2: Power extracted by turbines from a free, unconstrained, tidal current

$$P_t = ½ \left(0.315\right) \left(1000 \frac{kg}{m^3}\right) (0.3\, m^2) \left(1.5 \frac{m}{s}\right)^3$$

$$P_t = 141.75W$$

This means that, should the device run at the two efficiencies discussed above, then theoretically, the total power output, P_t, should be 141.75 W. If the device was inserted into free flowing water which averaged 1.5 m/s for a 24 hour day, then the total energy produced, E_t, that day would be 3.402kWh.

$$E_t = P_t \times t$$

$$E_t = (141.75W)\,(24\,hours)$$

$$E_t = 3.402kWh$$

Comparing the estimated power output of the device to other forms of alternative energy helps to give an idea as to the usefulness of 141.75W. A typical solar PV module can output between 10W and 300W (Energy, 2012). Assuming 5.5 hours of sunlight per day, this means that the energy output of a solar module can vary between 1.65kWh and 55kWh per day. Connect several solar modules together in series and a typical solar PV installation can supply 4 kWh or more. Should the device work as assumed, the power output of the generator device is comparable to a small solar PV installation and therefore useful.

LOAD-LINE ANALYSIS

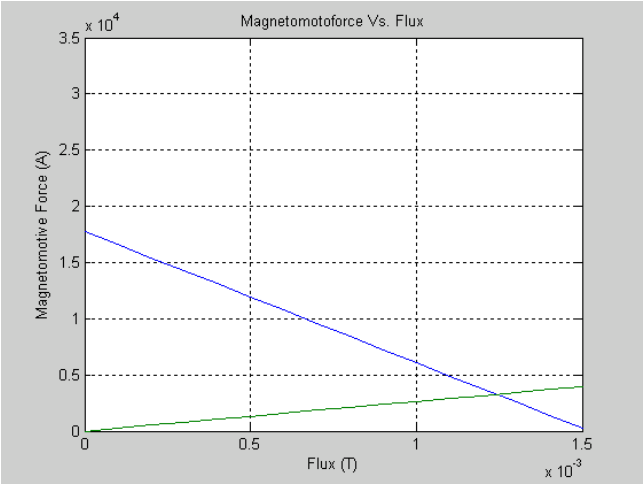

Figure 33: MATLAB Load-Line Analysis for the Alternator

In order to determine the feasibility of the design, MATLAB was utilized to analyze the operating point of the alternator. The operating point of the load-line analysis is represented by the intersection of the magnetomotive force line of the alternator, F_1, and the magnetomotive force line of the source, F_2. In Figure 33, the blue line represents the magnetomotive force of the alternator and the green line represents the magnetomotive force of the source. The lines in the graph are represented by the equations below.

$$\mathrm{F_1} = (\mathrm{H_m} \times \mathrm{L_m}) - \frac{(\mathrm{H_m} \times \mathrm{L_m})}{(\mathrm{B_r} \times \mathrm{A_m})} \times \phi_g \text{ (Blue)}$$

$$\mathrm{F_2} = (R_g + R_c) \times \phi_g \textit{ (Green)}$$

$$R_g = \frac{L_g}{\mu_o \times A_g}$$

$$R_c = \frac{L_g}{\mu_o \times \mu_r \times A_c}$$

The magnetomotive force of the source is calculated by multiplying the flux density of the air gap, Φ_g, with the reluctance of the circuit. The reluctance of the circuit was simplified to include the reluctance of the air gap, R_g, and the reluctance of the rotor core, R_c. The reluctance of the rotor core is much smaller than the reluctance of the air gap, which is the major source of resistance in the circuit.

$$\Phi_g = \int B_g \cdot dA_g$$

Equation 3: Definition of Magnetic Flux

$$\Phi_g = B_g \times A_g$$

$$1.2mT = B_g\,(0.001206m^2)$$

$$B_g = 0.995T$$

Utilizing the MATLAB analysis, the x-intercept of the operating point was found to be 1.2mT. With the magnetic flux in the air gap, Φ_g, and the cross-sectional area of the air gap, A_g, both known, the magnetic field in the air gap, B_g, was calculated to be 0.995T. One assumption made during this calculation was that the air gap area, A_g, is equivalent to the area of the permanent magnet, A_m. Additionally, we only took into account the magnetic flux that protrudes directly from the surface of the magnet, as shown in Figure 34 below.

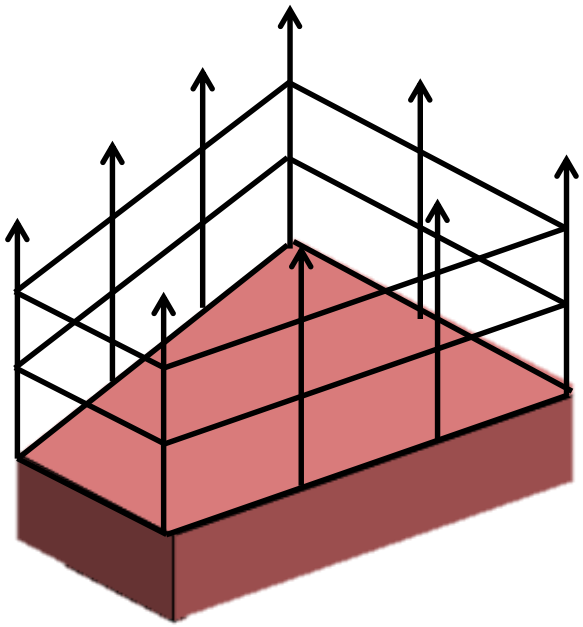

Figure 34: Flow of Magnetic Flux from the Permanent Magnets

$$\varepsilon = B_g \times l \times v \times N_{turns} \times 2$$

Equation 4: Induced Voltage in a Coil of Wire

$$v = \omega \times r \ = \ 2 \times \pi \times f \times r$$

$$v = 2.07 \frac{m}{s} \ at \ 180rpm$$

$$l = 0.04m$$

$$N_{turns} = 30$$

$$\varepsilon = (0.995T)(0.04\text{m}) \left(2.07 \frac{m}{s}\right) (30)(2)$$

$$\varepsilon = \ 4.94V \ per \ coil$$

$$\boldsymbol{\varepsilon = 19.77V \ per \ phase}$$

The induced voltage, Ɛ, is found by utilizing Equation 4. The velocity, v, of the magnet over the coil is calculated by multiplying the angular velocity, ω, and the radius to the center of a coil. The length of the coil, l, was assumed to be the length of the magnet side and each coil had 30 turns. Using the calculated magnetic field strength in the air gap, the induced voltage per phase is calculated to be 19.77V per phase. The induced voltage and the estimated power are then used to calculate the maximum anticipated current in the windings.

$$P = V \times I$$

$$141.75W = 19.77V \ \times I$$

$$\boldsymbol{I = 7.17A}$$

The calculated current of 7.17A is less than the 18A maximum current value, and will not cause any heat issues. The higher the current in a wire, the higher the temperature of that wire. This is due to the friction between the moving electrons in the conductor.

The following MATLAB analysis has been updated with current information, but contains the same procedure as when originally conducted.

$B_r = Magnetic\ Field\ Strength\ of\ Magnet\ (T)$
$B_g = Magnetic\ Field\ Strength\ in\ Air\ Gap\ (T)$
$A_m = Area\ of\ Magnet\ (m^2)$
$H_m = Coercivity\ of\ Magnet (MA/m)$
$L_m = Thickness\ of\ Magnet\ (m)$
$\mu_o = Permeability\ of\ Free\ Space$
$L_o = Thickness\ of\ Air\ gap\ (m)$
$A_g = Area\ of\ Air\ gap\ (m^2)$
$B_c = Remanence\ of\ Core (T)$
$H_c = Coercivity\ of\ Core (A/m)$
$\mu_c = Permeability\ of\ Core$
$L_c = Thickness\ of\ Core\ (m)$
$A_c = Area\ of\ Core\ (m^2)$
$R_c = Reluctance\ of\ Core\ (\Omega m)$
$R_g = Reluctance\ of\ Gap\ (\Omega m)$
$F_1 = Magnetomotive\ Force\ of\ Alternator$
$F_2 = Magnetomotive\ Force\ of\ Load$
$\phi_a = Air\ gap\ Flux\ Density\ (T)$

```
Br = 1.26;
Am = 0.001206;
Hm = 8.75 * 10^5;
Lm = 0.02032;
Uo =(4*pi*(10^-7));
Lg = 0.004;
Ag = Am;
Bc = 1.05;
Hc = 47.75;
Ur = Bc / Hc;
Lc = 0.0005;
Ac = (pi * 0.1524).^2;

Rc = Lc / (Ur * Uo * Ac)
Rg = Lg / (Uo * Ag)

Flux = 0:0.0001:0.002;
line1 = (Hm * Lm) - ((Hm * Lm) / (Br
* Am)) * Flux;
line2 = (Rg+Rc) * Flux;

idx = find(line1 - line2 < eps, 1);
px = Flux(idx)
py = line1(idx)

figure
plot(Flux, line1, Flux, line2)
title('Magnetomotoforce Vs. Flux');title('Magnetomotoforce Vs. Flux');
axis([0 .0015 0 35000]);
xlabel('Flux (T)');
ylabel('Magnetomotive Force (A)');
grid on;

Rc =
    0.0992

Rg =
   2.6394e+06

px =
    0.0012

py =
   2.5690e+03
```

TURBINE DESIGN

TURBINE POWER

The turbine was design for optimal performance with the sixteen magnet axial flux alternator used in the machine. Utilizing the approximately 1ft diameter for the turbine, the team calculated an approximate rotation speed for the output of the turbine blade. The speed of the current was assumed at 1.5 m/s.

$$d = 12in = .3048m$$

$$C = .957m$$

$$v = 1.5\frac{m}{s}$$

$$v/C = 1.57rps = 94rpm$$

As the above calculation shows, a current speed of 1.5 m/s outputs rotation at about 94 RPM. This number though is for a drag based device. As the turbine utilized features hydrofoil shaped blades, the turbine will actually produce a positive lift force when acted upon by the current rather than only passive resultant force. This would yield a slightly higher output speed, estimated to be between 100 and 120 RPM.

BLADE MODELING

Since the turbine is designed for use in submerged applications, the project team sought to determine a blade profile that would perform ideally under these conditions. As a product of background research, the group found an optimized hydrofoil profile for low head, low velocity applications reported by the School of Mechanical Engineering Shanghai China (Yang). A picture from the report showing the optimized hydrofoil shape, as compared to the standard NACA0012 foil is shown below. Further information regarding the optimized hydrofoil results can be found in the report by Yang, found in the References section of the report.

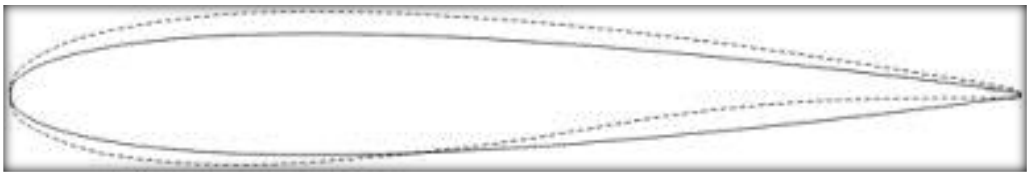

Figure 35: Comparison of Optimized Hydrofoil (NACA0012 airfoil = solid, optimized airfoil = dashed)

In order to utilize this hydrofoil profile, the project team had to recreate the shape in the solid model which would then be used to rapid prototype the helical blades. The process that was used to do this required several steps in order to effectively approximate and recreate this shape. First, Figure 35 above was printed out onto graph paper. Then, coordinate points for an NACA0012 were obtained from the UIUC Airfoil Coordinate Database and these data points were superimposed onto the graph of the two profiles. Then, using the graph paper in combination with the known data points, new data points were placed at about fifty locations along the optimized profile and their corresponding coordinate values approximated. These data sets were then input into Microsoft Excel in two groups, one for the top and another for the bottom. Using these data sets in Excel, a best fit 6th-order polynomial function was generated for each and the equation was recorded. Once these equations were obtained, they were able to be imported into SolidWorks as equation-driven curves. After both curves were combined and converted into editable sketches, they were scaled to the appropriate size of approximately 10 cm in length. This sketch was then further manipulated to model the helical blades used in the design.

In order to ensure that the recreated blade profile geometry retained a hydrodynamic benefit, the obtained profile's performance was simulated. This simulation was completed using computational airfoil simulation software called XFLR5. The simulation environment was set up to approximate the results based on the fluid flow of water for a low Reynolds number. As the simulation results demonstrate, the generated profile functions as a hydrofoil. The performance of the hydrofoil can be seen in the graphical analysis, as compared to the NACA0012 profile. The inconsistencies seen in the simulation are the result of the geometry approximation and are not indicative of performance losses.

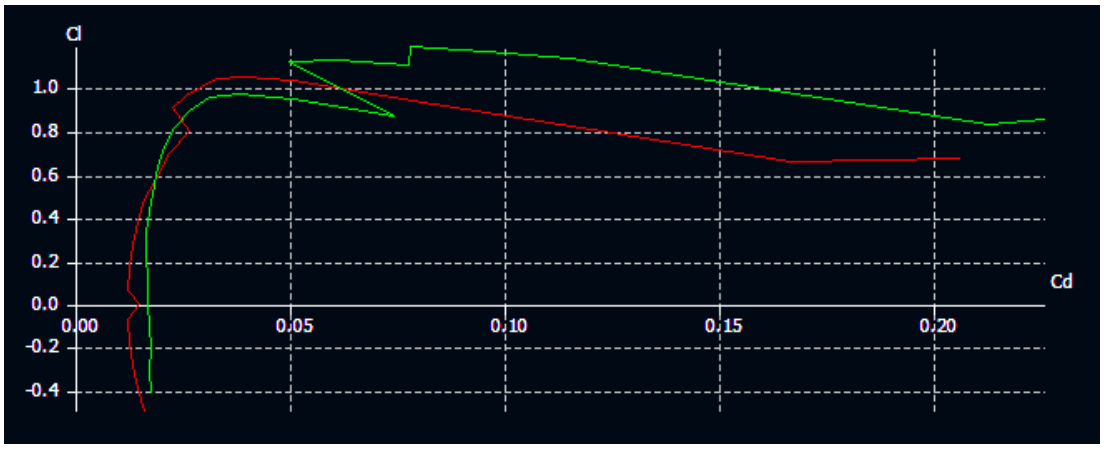

Figure 36: Lift Coefficient vs. Drag Coefficient of Optimized Hydrofoil and NACA0012 Profile

As Figure 36 shows, the recreated geometry (green) was able to create more lift than the NACA0012 (red) profile for most conditions. This result indicates that for higher speed or turbulent flow scenarios, the optimized geometry would accelerate more than the NACA0012 shape. In low drag scenarios, the hydrofoil's geometry's performance is about on par with the NACA0012 shape, indicating a better overall performance and endorsing the application of the geometry for this project.

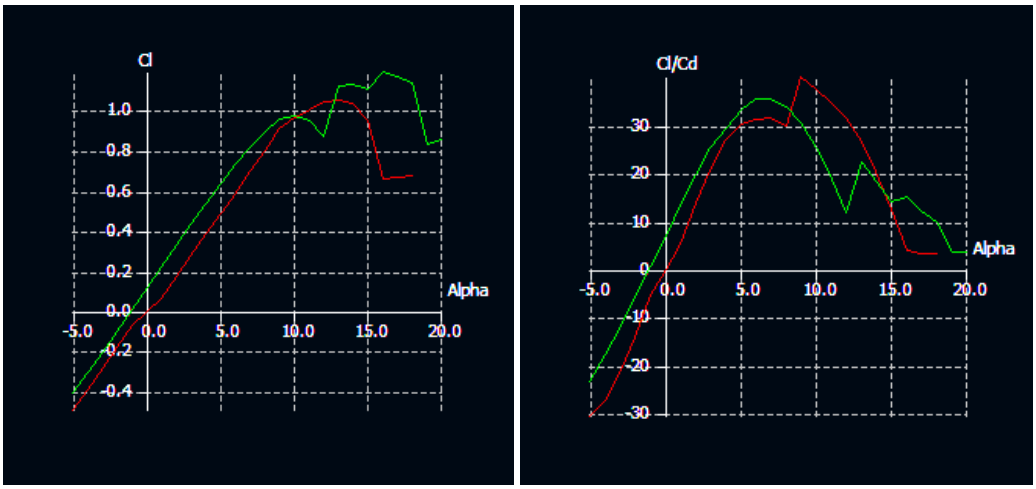

Figure 37: Coefficient of Lift vs. Angle of Attack (Left), Glide Ratio vs. Angle of Attack for Optimized Hydrofoil

Further simulation results can be seen in Figure 37. The graph on the left shows that for most angles of attack, the hydrofoil (green) creates more lift than the NACA0012 profile (red). This is key in the application of the hydrofoil in this machine, as the helical turbine presents the hydrofoil across a range of angles of attack simultaneously. Across this range of angles of attack the hydrofoil geometry generates more lift than the

NACA0012 indicating its effectiveness in this application. The graph on the right shows the simulation results for the two geometries for their glide ratio (Cl/Cd) as compared to the angle of attack. For this factor, the hydrofoil geometry again outperforms the NACA0012 across a range of angles of attack. The glide ratio indicates the respective geometry's ability to maintain speed (glide) and the hydrofoil's performance again indicates that it is effective for application in the machine's helical turbine.

BLADE MATERIAL SELECTION

While selecting materials for use in the helical turbine, the project team considered several options. Some of the considered materials were aluminum, wood, steel, and several plastics. A design matrix showing several materials and important considerations for the materials is shown in Table 4 below:

Table 4: Design Matrix for the Selection of Turbine Blade Materials

Material	Cost	Strength	Weight	Manufacturability	Total
Influence	0.4	0.15	0.15	0.3	
Aluminum	3	8	3	2	3.45
Wood	5	6	5	4	4.85
Steel	2	9	2	2	3.05
ABS	6	5	8	10	7.35
PLA	8	4	8	10	8

As the design matrix shows, the two most important factors in choosing a material were the cost of the material and the ability to manufacture the material into helical blades. Aluminum, steel, and wood all require a large piece of stock in order to produce the helical shape. These methods are also cumbersome and leave much potential for error. In the case of ABS and PLA, both materials would be utilized via a rapid prototyping machine making them much more easily created as well as being considerably cheaper. The drawbacks with material strength were remedied by pouring the blades in fiberglass resin in order to obtain a sturdy waterproof set of blades.

TURBINE 3D MODELING

After multiple failed efforts to use equations to draw the profile sketch the team imported the optimized profile image from its corresponding report into SolidWorks and traced a spline over it as close as possible. This spline was then used as the profile to build an individual helix blade wrapping 1/3 of the turbine's rotational path circumference. The blade then featured an inward sweep toward the rotational axis. Into this face was placed a female acceptor slot for the strut plate male end to mount each blade into the turbine assembly.

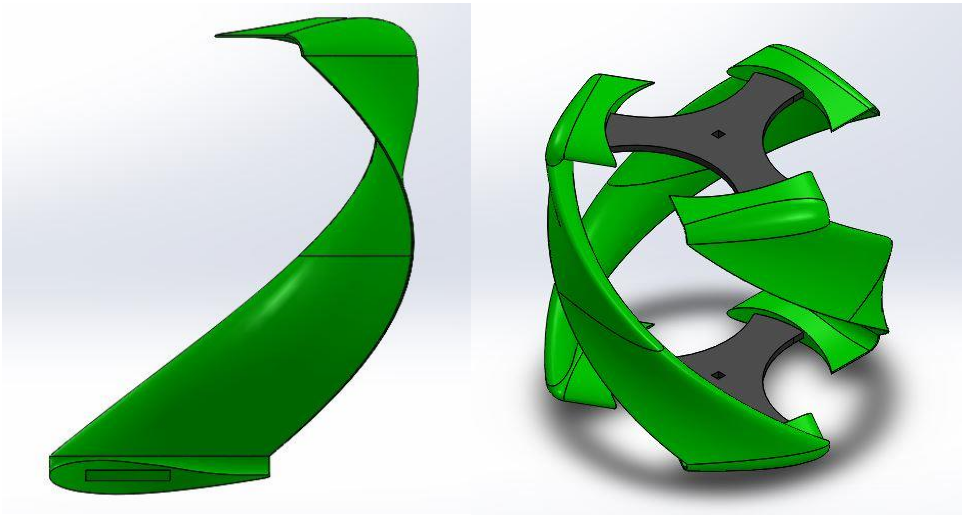

Figure 38: Gorlov Helical Turbine and Blade SolidWorks Model

FRAME DESIGN

The frame was the dependent design component variable. Based on the modifications to the alternator components the frame was accordingly redesigned to fixture the blade assemblies and alternator into a single unit.

FRAME MATERIAL SELECTION

For the frame, two materials are used for the majority of the design. The vertical members are made of two steel rods that run 3ft in length up two sides of the device. The four horizontal cross members are made of high density polyethylene.

The materials listed above were selected for a combination of reasons. The steel was selected because it could provide more than enough strength to keep the frame sturdy. In addition to its strength, though, the steel rod was available at an economical price. The round rods also present an advantage in that they will allow a much more laminar flow as compared to a prismatic geometry, allowing water to flow between the rods as opposed to around the outside of them, which will contribute to giving the turbine a slightly more balanced omnidirectional functionality.

The HDPE was selected for the cross members for similar reasons. First, the cost of HDPE as compared to aluminum or steel is considerably low. This was a large motivating factor for choosing HDPE as a material for the cross members. In addition to its price, HDPE is also an easier to manufacture plastic making it ideal for use in this application as the part geometry requires some CNC work. HDPE also presents an advantage over other plastics like LDPE and PLA in that has much higher yield strength. This yield strength advantage is important as these pieces comprise the frame of the machine and must be able to withstand significant external forces without deformation.

As this model is a prototype, not all of the materials used would be ideal for larger scale applications. In particular, the HDPE would likely be switched with a material that would be more easily machined and form a more efficient seal. This material could still be plastic, like a marine grade ABS, or could be metal, like aluminum or stainless steel. It is important to consider this, however, as salt water will induce corrosion upon a material much more quickly than other non-saline liquidus fluids or gaseous air.

FRAME 3D MODELING

The final frame design consists of four steel circular rod supports and a set of two different high density polyethylene joining blocks, one set for each side of the alternator. Each of the four HDPE frame components feature press fit bearing and fluid seal fixturing slots. The model also includes hardware features and the modular link brackets on both ends. Figure 39 shows the SolidWorks model of the frame.

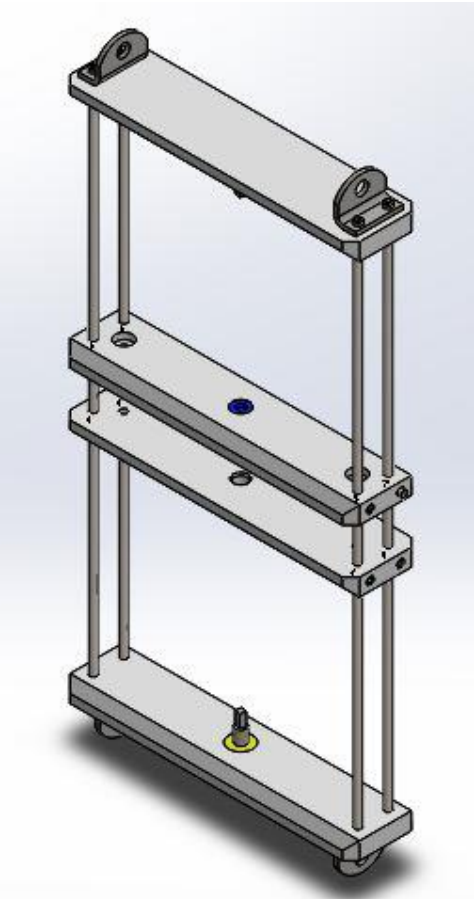

Figure 39: Frame Modeled in SolidWorks

GENERATOR DESIGN ITERATIONS

The evolution of the design is best shown through the illustrations and descriptions of the design iterations developed throughout the process. Each iteration was an improvement or modification from the previous design based on new research and analysis. A summary of the key design choices can be found in the subsequent section.

ITERATION 1

This was the first iteration of the machine model. The machine is horizontally symmetrical and about 2ft tall and 1.5ft across (.6m tall x .45m wide). The helical turbine is 1ft in diameter (.3m), with three blades at an aspect ratio of 2:1. This design features two axial-flux alternators built around the outside circumference of the turbine's top and bottom cap plates. The magnet rotors were to be multipurpose, acting as alternator rotors as well as the circular mounts of the turbine blades. The machine was built into a vertically split, two pieced frame. The frame ends features a 2:1 groove joint with a through hole, acting as a modular "chain link" connection.

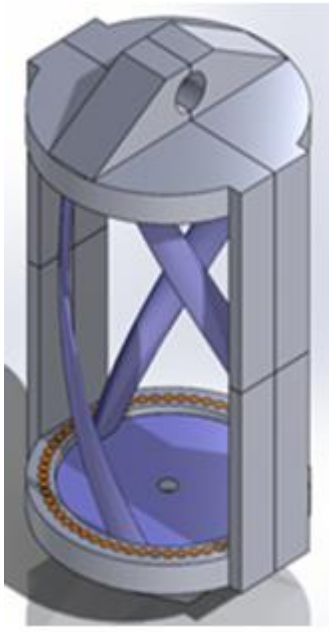

Figure 40: Iteration 1

As this was the first design iteration, there were several problems that were quickly foreseen and addressed. Difficulties including the ease of manufacturability, environmental exposure, and reduction of costs lead us to the next design.

ITERATION 2

In this design, the axial flux alternator was modeled in several disk layers that could be assembled in stacks. This design featured two identical top and bottom alternators held together using side bars serving as a frame to provide structural support to the alternator. A three blade helical turbine similar to that of the first iteration would sit inside these alternators and their frame. These blades would mount on plate fixtures, as before, or would be on individual arms as shown on the left side of Figure 41. This turbine component would mount to the alternator on the axles coming out of the alternator housing.

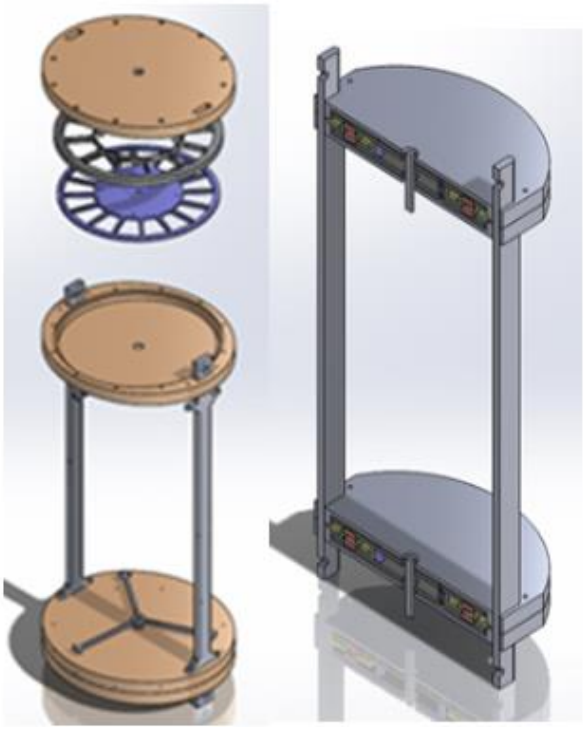

Figure 41: Iteration 2

The alternator features a thin stator disk with 12 internal coils. The stator would then rest on a small lip in order to suspend the stator coils between the dual magnet rotors. The rotating turbine would transfer the motion to the alternator rotors on both sides subsequently creating power. This second design iteration was further developed to account for available and affordable materials.

ITERATION 3

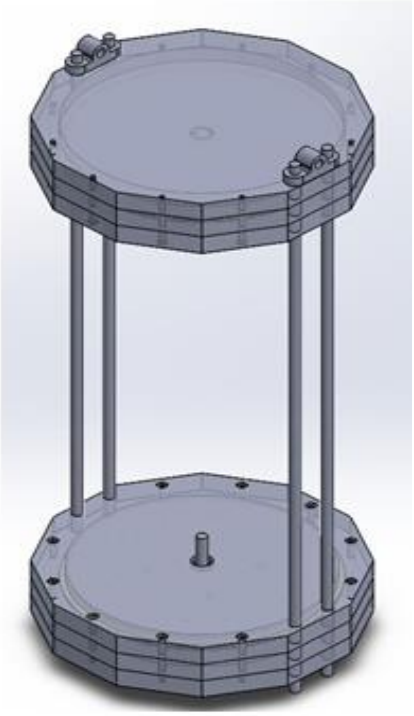

Figure 42: Iteration 3

This model was redesigned based on research of attainable materials. In order to reduce costs, components were redesigned to be in better accordance with the shapes and sizes readily available and modifiable. The frame design that was featured in the previous iteration was replaced here for cost reasons using two steel rods with threaded ends in place of the plate bars on each side.

The alternator remained wholly unchanged regarding its inner components, however, the housing was redesigned. The redesign featured a slight change in geometry, changing from an ovular shape to an octagonal one. The geometric redesign was done to facilitate fixturing of any external components to the now flat sides. These alternator housing pieces were modeled using pieces of 14in x14in x1in (.36m x .36m x .3m) high density polyethylene (HDPE) plate stock.

ITERATION 4

This design iteration saw the most significant changes compared to the previous three iterations. This model features a single alternator instead of two. This is a key component of the redesign as it greatly decreased the cost and effort of manufacturing. Additionally, the large 2ft blade setups were split into two separate 1ft blade sets. The group decided to 3D print the hydrofoil blades for ease of manufacturing. Of the available 3D printers, we decided to utilize a MakerBot Replicator 2 due to its realistic usage cost and availability.

The frame's previous design consisted of four vertically oriented steel rods, running the length of the machine, which then connected to the alternator housing and created a rectangular frame. With the movement of the alternator and its housing, the twin alternator housings could no longer used to provide structural support to the machine. Instead, the structural support of the machine is provided by those same four vertical steel rods, now

connected to four metal cross members with the modular links built into them. These new frame plates provided a surface easily and securely bolt bearings onto.

This redesign isolated the structural components and separated them from the electrical components. This is an important piece of the design as in the prior iterations a structural malfunction or failure would lead to the destruction of the entire machine. With these changes the alternator housing or structural components can fail independently, leaving the other intact and able to be fixed or replaced on site.

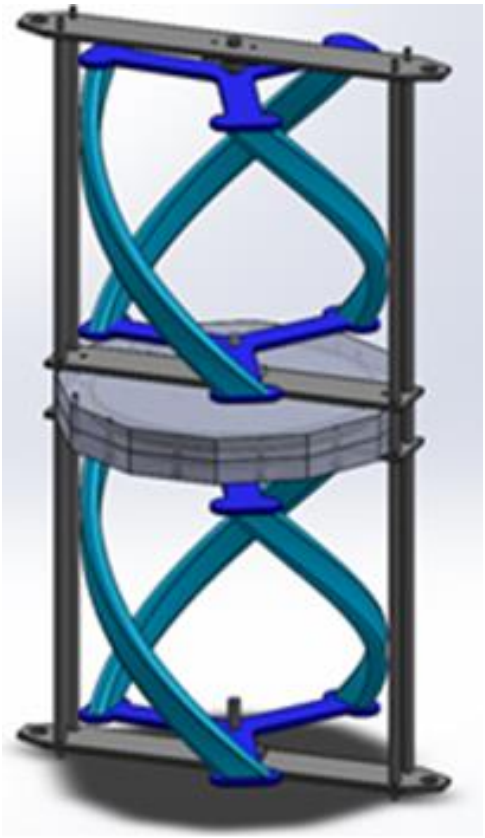

Figure 43: Iteration 4

The helical turbine was accordingly redesigned to fit with the model. The aspect ratio was adjusted to 1:1 maintaining full circumferential wrapping of the blades. This shorter version of the turbine is then utilized twice, once above and once below the alternator as previously discussed. The final blade mounting system was also chosen. Departing from the circular plate design originally used, as can be seen in the image above, each blade was mounted on a single plate with individual strut arms. The design of these strut plates significantly reduced the weight of the turbine assembly and made the blade-strut fixture straighter forward to assemble. These design changes helped maintain balance of the generator and significantly improved all aspects of the design.

ITERATION 5

This iteration of the design was made in order to finalize several aspects for the production of the machine frame. Due to expenses of metal and the available HDPE plate stock geometries it was found to be more effective to build the frame horizontals out of plastic.

This increased the overall machine length and bulk of individual frame components. The edges of the cross members were rounded so as to reduce excessive turbulence in the fluid flow around the blades. The increased cross member thickness also allows more versatility in the mounting of bearings and support rods.

The alternator housing was redesigned to feature a stator support disk separate from the alternator housing. This modification allowed the full stator to be assembled prior to integration into the rotor assembly. It also allowed for increased thickness allowances in the housing top and bottom.

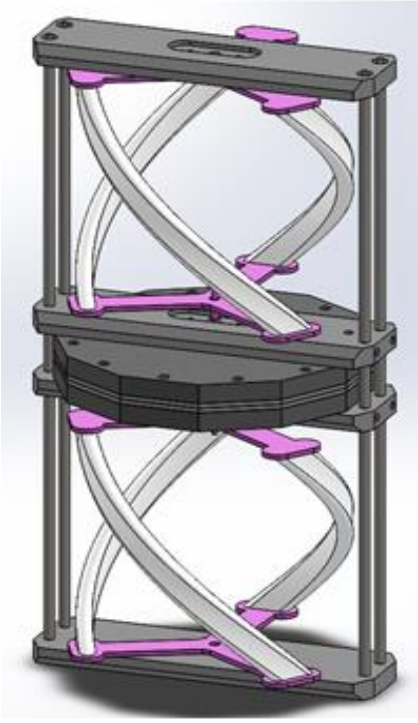

Figure 44: Iteration 5

ITERATION 6

In the further development of the machine, this iteration represents the final step in the design. In this iteration, the helical blades have been remodeled.

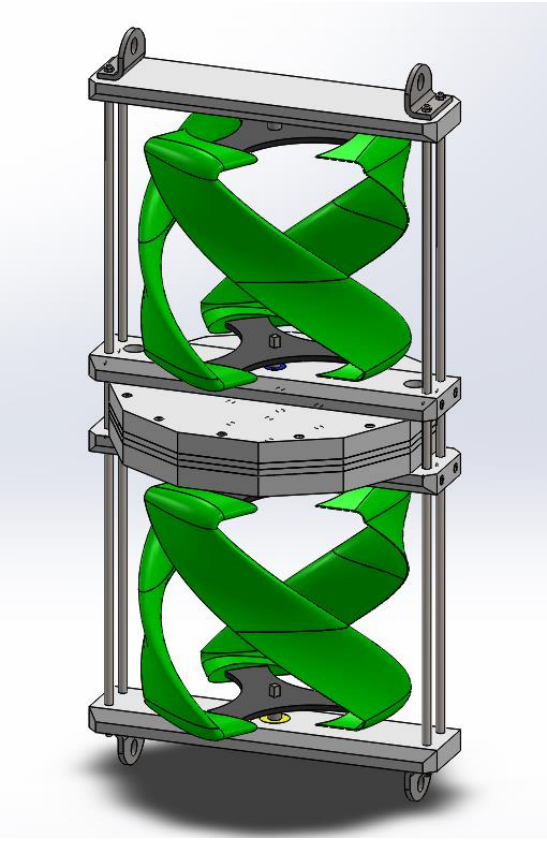

Figure 45: Iteration 6

The blades now are made of two separate pieces that will be attached together. This change facilitates the maximum manufacturing size with the MakerBot Replicator 2 3D printer. The blades in this iteration also have their terminating faces turned in toward the center axis for a convenient female connection point for the plate male strut ends.

The frame components in this design also feature press in radial bearings in all 4 frame cross members and a press fit seal in the center two cross members around the outermost ends of the axle. This iteration, apart from redesign, also includes updated solid models regarding some other device hardware. This includes nuts, bolts, washers, as well as the final modular link brackets.

PROTOTYPE MANUFACTURE

FRAME MANUFACTURE

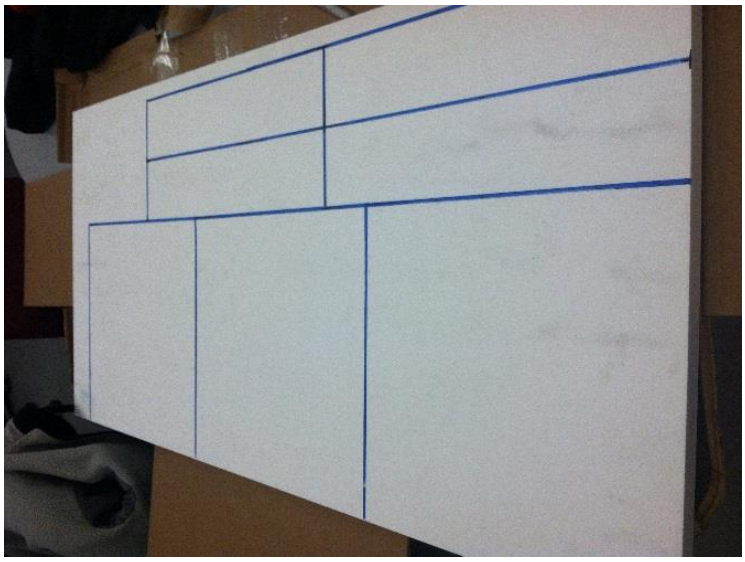

Figure 46: HDPE Stock

In order to manufacture the frame, the steel rods and HDPE cross members required some machining. The steel rods needed to be cut to length and turned down to a ¼in diameter. This was done using a CNC lathe. Then, the HDPE then was cut into appropriately sized blocks for the frame cross-members, and the alternator housing. The HDPE Stock is shown in Figure 46. These blocks were then milled in the Haas VF4 CNC Mill. The manufacturing of the HDPE pieces included several operations which rounded the edges, drilled the holes, and cut away several geometries that were incorporated into the piece for the assembly of the machine.

In order to produce several pieces for use in the frame construction, computer aided manufacturing profiles needed to be produced. The CAM profiles for the pieces were generated using the CAM software Esprit. The CAM profiles for the frame pieces included several pocketing operations, hole drilling and contouring to size.

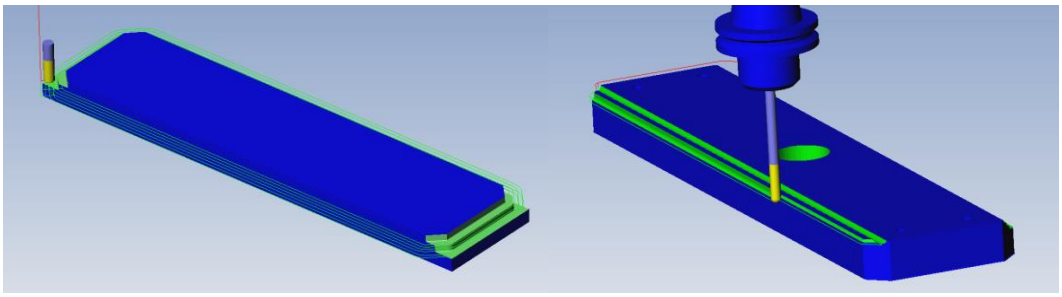

Figure 47: CAM Simulation in Esprit for Frame Piece Production

Two captures of the CAM simulation for one of the frame pieces can be seen in Figure 47 above. CNC machining was essential to use in order to produce consistent results within the specified tolerance, a task that would likely not be accomplished if the parts were hand produced. Finally the edges of the cross members were routed to a 45° angle to reduce turbulence of the water flowing through the turbine area.

TURBINE MANUFACTURE

The challenge that is frequently associated with the use of helical turbines is the difficulty of manufacturing the proper profile shape and the helical sweep necessary in the Gorlov design. Slight deformations in the blade shape can have a significant effect on the performance of the turbine. In order to get blades with the best possible geometry, the team elected to utilize rapid prototyping in order to obtain a consistent shape.

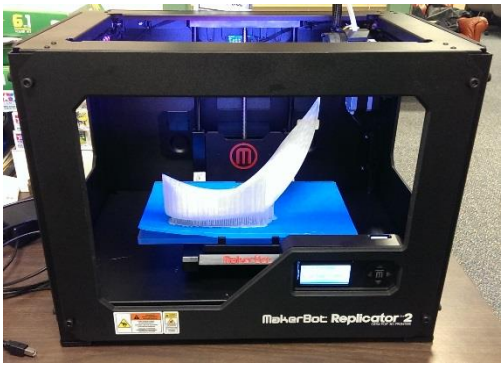

Figure 48: MakerBot 3D Blade Printing

The blades were first modeled in DS SolidWorks, as described in the turbine design section. The 3D part models, which included a profile for an optimized hydrofoil, were then 3D printed using a MakerBot Replicator 2 rapid prototype utilizing PLA as a material. This process can be seen in Figure 48.

Once the blades had been created, they were assembled by casting the plastic pieces in a fiberglass reinforced epoxy resin in order to increase its strength, stiffness, and durability of the helical blades. The porosity of the 3D printed PLA is too high to become a non-water permeable surface upon production. This fiber/resin casting is essential in allowing the rapid prototyped blades to maintain integrity and function underwater.

Figure 49: Assembled Helical Turbine

In addition to manufacturing the blades, the struts which hold the blades also needed to be produced. While this geometry is somewhat complex, the design is planar and therefore, it was able to be easily laser cut. This process is shown in Figure 50 below.

Figure 50: Laser Cut Struts for Blade Assembly

ALTERNATOR MANUFACTURE

The portion of the machine that required the most careful and accurate assembly was the construction of the axial flux alternator for the machine. The process required a very methodical approach in order to ensure safety, proper rotational freedom and rotational balance.

ROTOR

To start, a wood magnet locating mold was laser cut from the SolidWorks mode. The steel rotor plates were cleaned to remove any dirt or oils that were on the surface. Once the surface was cleaned the locating mold was bolted to the steel for the magnets to be perfectly aligned. The magnets were initially attached using JB Weld two-part metal adhesive.

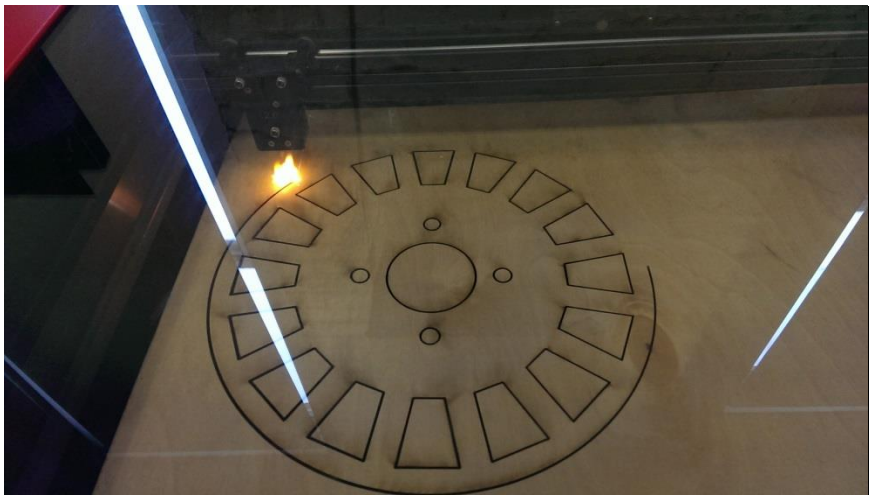

Figure 51: Laser Cutting of Wooden, Magnet Rotor, Assembly Frame

Before the magnets were attached they were also cleaned in order to remove any oils or dirt on the surface. Once the magnets were cleaned, the project team determined the orientation of the poles of each magnet. The poles were determined by comparing the magnets to each other and arranging them so that the poles alternated north and south around each rotor face. Once a magnet was clean and in the right orientation determined, it was slid into its corresponding slot in the wooden mold and clamped in place to allow the adhesive to cure. This process was done four magnets at a time until both, sixteen magnet rotors were complete.

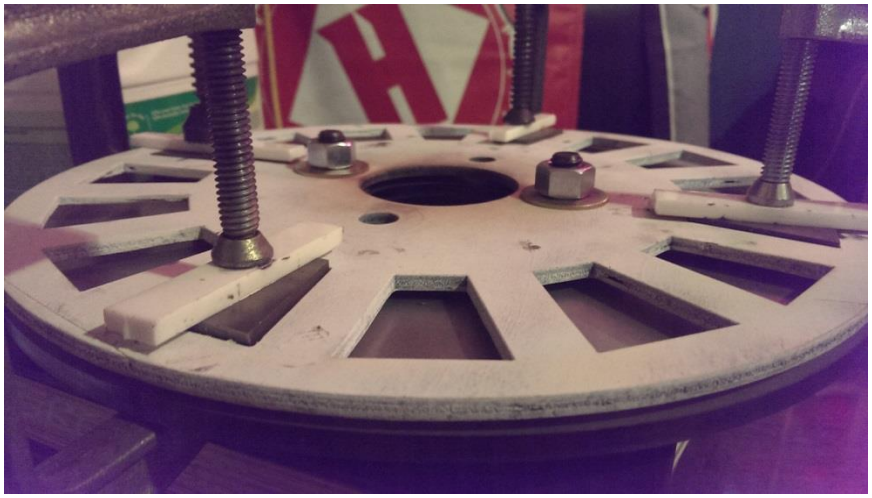

Figure 52: Assembly of a Magnet Rotor Plate

After the magnets were attached to the plates and the adhesive had completely dried, the project team needed to protect the magnets and improve fixturing without disrupting the magnetic flux. In order to do this, the magnet rotors were cast into an epoxy resin thermoset polymer. The resin mixture was poured in an O shape encasing the magnets but leaving the top perimeter edge and center face of the plate untouched. This fiberglass casing protects the magnets physically but still allows magnetic force to act. The directed magnetic force of the magnets was checked using view paper to ensure that the magnetic force was not reduced after the fiberglass was poured.

Figure 53: Magnet Rotor with Magnetic Field Paper Showing Magnetic Field

STATOR

Aside from the construction of the magnet rotors, a twelve coil stator needed to be created in order to harness the energy of the moving magnetic pole pairs. In order to create coils of the exact size used in the solid model, an assembly method was devised that could be consistently replicated. This method utilized a small acrylic center piece, two steel plates, a bolt, nuts and washers. The small acrylic piece was laser cut utilizing the same method as the wooden magnet rotor frame. The thickness of acrylic piece was the intended thickness for our magnet wire coils, or 3mm. Exactly 30 turns of magnet wire was wound around the acrylic core, while epoxy resin was poured and brushed onto the wire. The fiberglass set after 2 hours and the coils could be removed for inspection and subsequent use in the stator.

Figure 54: Coil Production Setup

The coil production setup for the stator design is pictured above in Figure 54. Once the twelve coils were made, they needed to be set in place. This was done using the same method as the magnets in the rotor. The coils were arranged to their ultimate orientation on a laser cut template mold and then epoxy resin was poured around them. Once the resin had dried, one solid disk enclosing twelve copper coils was left.

This stator disk then needed to be appropriately wired and soldered into a 3-phase configuration. A picture of the stator in this state can be found in Figure 55. Once the magnet rotors and stator disk were created, the final step to the completion of the alternator was the assembly of the component pieces. Several figures depicting the assembly of the alternator can be found below.

Figure 55: Stator Before and After Fiberglass Resin Poor

AXLE

Overall the generator has three axles, two small axles mounted on the outer machine ends for turbine rotation only as well as one center axle for alternator rotation. The center axle was built to maintain insulation from the magnetic field while serving as the backbone of the entire alternator. This steel axle had a HDPE centering core mounted at its center, was turned down for two press fit bearings and seals, and milled square at the ends for turbine mounting. This centering core acted as the insulating connector between the metallic axle-bearing assembly and the metallic rotor. Figure 56, below, shows the SolidWorks models for the assembled alternator and the axle core.

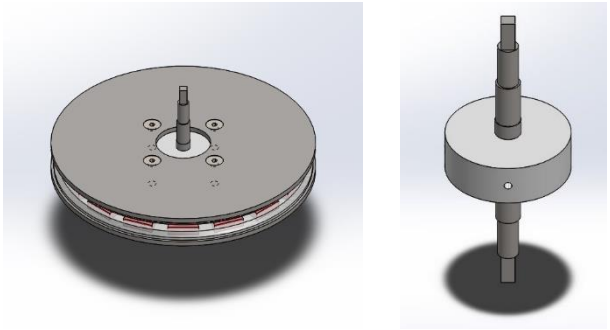

Figure 56: Assembled Alternator and Alternator Core Models in SolidWorks

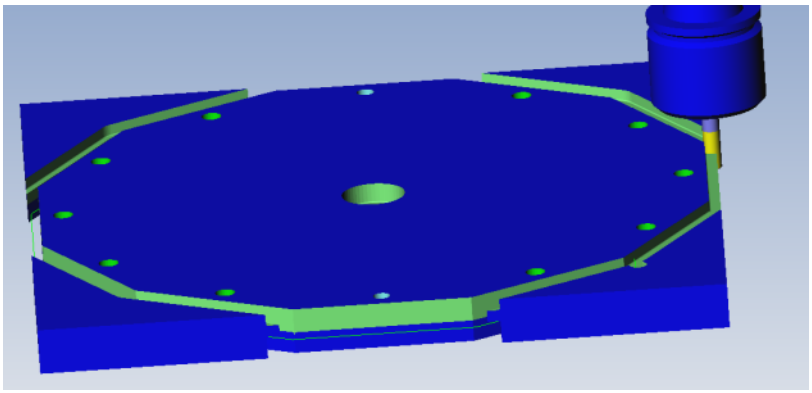

Figure 57: CNC Cutting Simulation for Alternator Housing

Beyond the functional components of the alternator, there were additional pieces that required CNC production. The housing for the alternator and the stator mount disks required a CAM profile be made. The manufacture of the pieces included a pocketing operation in which the alternator ultimately sits. The housing CAM profile of the machining for these pieces can be seen in Figure 57, above.

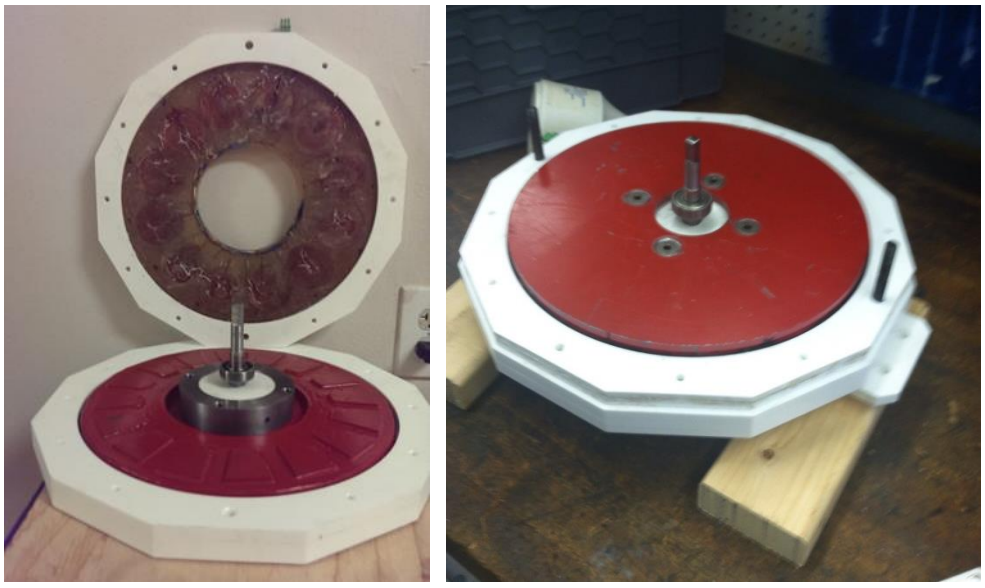

Figure 58: Final Stages of the Alternator Assembly

TESTING AND RESULTS

A key aspect of the MQP project is to compare anticipated outcomes to measured results. Through the testing of our device, the team verified the capabilities of our design. The alternator was tested as a separate unit in a dry environment and then again in the assembled device in the crew tank. Dry tests were performed in the electrical engineering labs and focused on the functionality of the alternator, making sure lab equipment could trace voltage and current waveforms to confirm the device could output power as expected. Afterwards, the fully assembled device was submerged in the crew tank and focused more on the turbine functionality, watertight capabilities, and signs of possible structural deterioration. The final prototype used for all testing procedures is shown below:

Figure 59: Fully Assembled Generator Device

PROCEDURE

In order to test the components of the device independently, the most complex piece (the alternator) was tested first in lab. During testing, the group built a device that utilizes a variety of gearing assemblies extracted from a 10-speed bike to manipulate a single-speed 30 RPM electric motor. The testing device easily allowed for adjustment between output speeds and for the alternator to be tested multiple times across a number of consistent conditions. The alternator with the testing equipment in the electronics lab can be seen in Figure 60 below. Using this device, the project team measured the voltage-current waveforms created by the alternator using multiple input speeds and gathered output values for current, voltage, and power.

Figure 60: Alternator Dry Testing Setup

In addition to testing the performance output of the alternator, the group also saw it necessary to determine several other characteristics regarding alternator independence from machine performance. The most important of these was a measured resistance of the coils in the machine. All of the experimental data for these tests can be found in the Results section of the report.

Following the dry tests, which confirmed the working nature of the alternator, the project team tested the machine in the rowing tanks at WPI's Recreation Center. The rowing tanks were utilized because they were

able to produce a steady stream of current flow across a range of speeds. Once the alternator was sufficiently sealed and prepared for underwater tests, the team began the process of testing in the rowing tanks. A picture of the test preparations can be seen above in Figure 61.

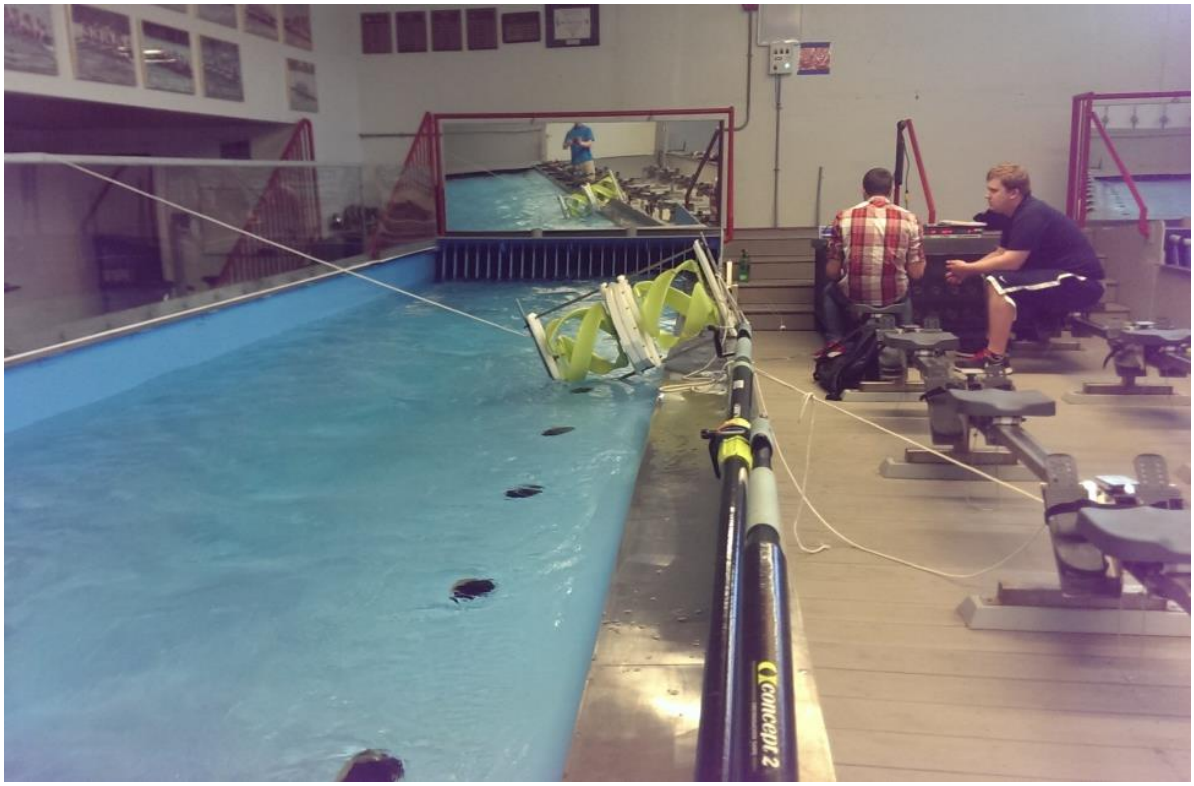

Figure 61: Preparing for Underwater Testing

The first step was to assemble the necessary materials for the test. If something were to go wrong, our device was at risk of damage. These preparations included gathering rope and masking tape for securing the generator, data recording devices (i.e. stopwatch, notebooks, etc.), three variable resistors, and an oscilloscope and digital multimeter to read electronic outputs. Once the resistors were all set to the same values wired in the primary circuit, the device was carefully lowered into the tank, as seen in Figure 61. Rope tied to both sides of the generator were used to anchor it down and setup so that they could be easily re-tensioned at higher flume speeds.

The next step was to setup a series of distance markers so that a flume speed could be gathered for each trial. This was important since the room speed controller did not automatically relate speed to engineering quantities. Masking tape was placed every foot for a 15ft margin and marked accordingly, as shown in Figure 62 below. A small floating device would be dropped in before the zero marker, and timed in the length of time it took to travel from 0ft to 15ft. This was repeated several times for each trial so the times could provide an accurate average flume speed in ft/s.

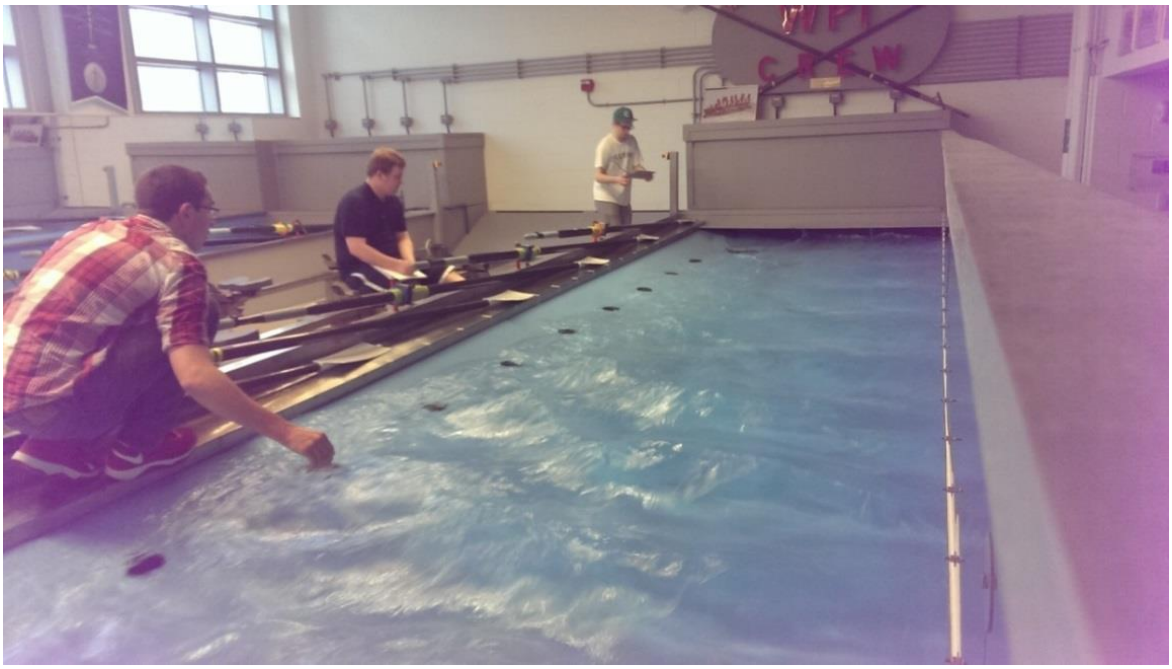

Figure 62: Measuring the Flume Speed

Once these flume speeds were recorded, a measurement of RPM was needed. To do this, the project team marked one of the helical blades with a thick, dark mark. Then, the amount of time it took the turbine to spin for 10 revolutions was gathered. Using these times, an approximate measurement of RPMs for the turbine could be approximated. Finally, once the device had been spinning at a constant speed, the voltage, amperage, and wattage were recorded. This was done for each of the trials at a resistance of 20Ω and later repeated at 5Ω. One trial was obtained at 3.7Ω at maximum flume speed to confirm a greater power gain. The data sets for the 20Ω and 5Ω trials can also be found in the Results section of the report (see next section).

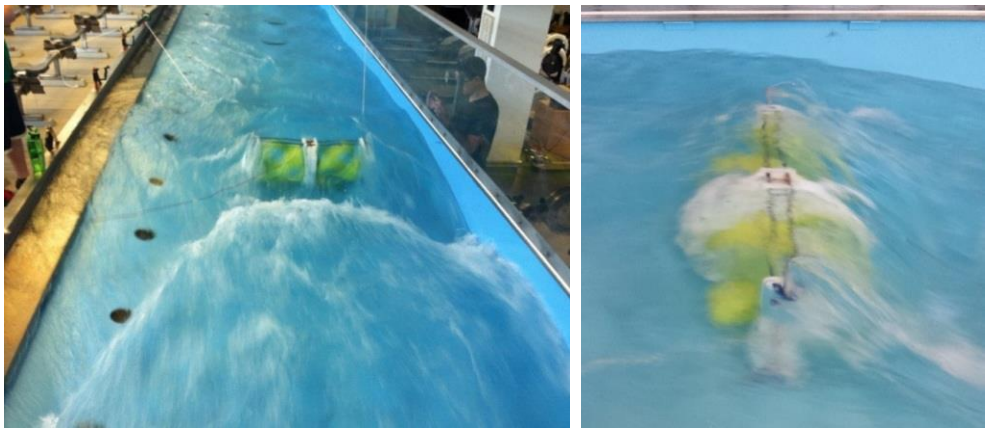

Figure 63: Underwater Testing with Moving Water Current

Figure 63 above shows the generator fully submerged and working as expected. The rope fixture and metal clamps on both sides of the generator housing prevented the device from swaying or falling over. At first, there was some complications with getting the blades to spin, but the problem was soon determined to be an issue with the center axle being too tight. Needless to say, even at top speed, there was little troubleshooting required. After the tests concluded, the team vertically orientated the device to see how fluid flow would move the lower half of the turbine. While not as efficient as the horizontal orientation, mostly due to half of the turbine sticking out above the surface, it did adequately prove that the team's generator design could be suitable for almost any underwater applications.

DRY TESTING RESULTS

The data that was obtained during dry testing of the alternator at two resistance values is summarized in the tables below. Readings of the RPMs, voltage, current, and power were recorded for a 10Ω and 51Ω configuration. As expected, the results of both load configurations show that the current, voltage and power increase as the rotation speed increases.

Table 5: Dry Test Results at 10Ω

R = 10Ω				
Gear	**RPM**	Iac (A)	Vac (V)	**P (W)**
NA	**0**	0	0	**0**
2-1	**31.875**	0.175	1.770	**0.310**
1-1	**39.375**	0.213	2.200	**0.469**
2-2	**42.500**	0.209	2.070	**0.433**
2-3	**51.000**	0.231	2.350	**0.543**
1-2	**52.500**	0.250	2.550	**0.638**
1-3	**63.000**	0.290	2.900	**0.841**
1-4	**70.000**	0.337	3.400	**1.146**
1-5	**78.500**	0.375	3.800	**1.425**

Table 6: Dry Test Results at 51Ω

R = 51Ω				
Gear	**RPM**	Iac (A)	Vac (V)	**P (W)**
NA	**0**	0	0	**0**
2-1	**31.875**	0.035	1.840	**0.064**
1-1	**39.375**	0.043	2.280	**0.098**
2-2	**42.500**	0.044	2.180	**0.096**
2-3	**51.000**	0.044	2.460	**0.108**
1-2	**52.500**	0.049	2.600	**0.127**
2-4	**56.667**	0.054	2.820	**0.152**
1-3	**63.000**	0.059	3.010	**0.178**
1-4	**70.000**	0.067	3.500	**0.235**
1-5	**78.750**	0.076	4.000	**0.304**

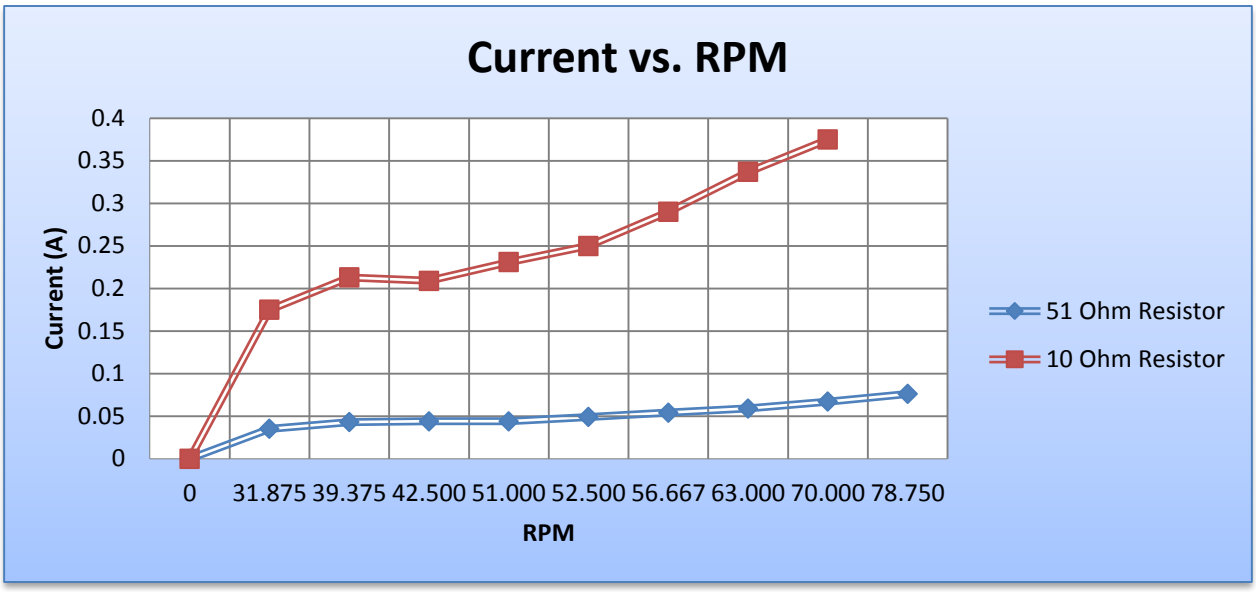

Figure 64: Current vs. Rotations per Minute (Dry Testing)

Figure 64 (above) is a graph of the current as a function on RPM. As expected, the current increases as the turbine rotated faster. This can be derived from the following equation: To convert rotations per minute to rotations per second, ƒ, simply divide the RPM value by 60. As ƒ increases with B_r, l_m, and N_{turns} remaining constant, the induced voltage, Ɛ, increases. The increase in the induced voltage results in an increase in power and current. Figure 65, below, shows how the voltage expectedly increases with respect to rpm.

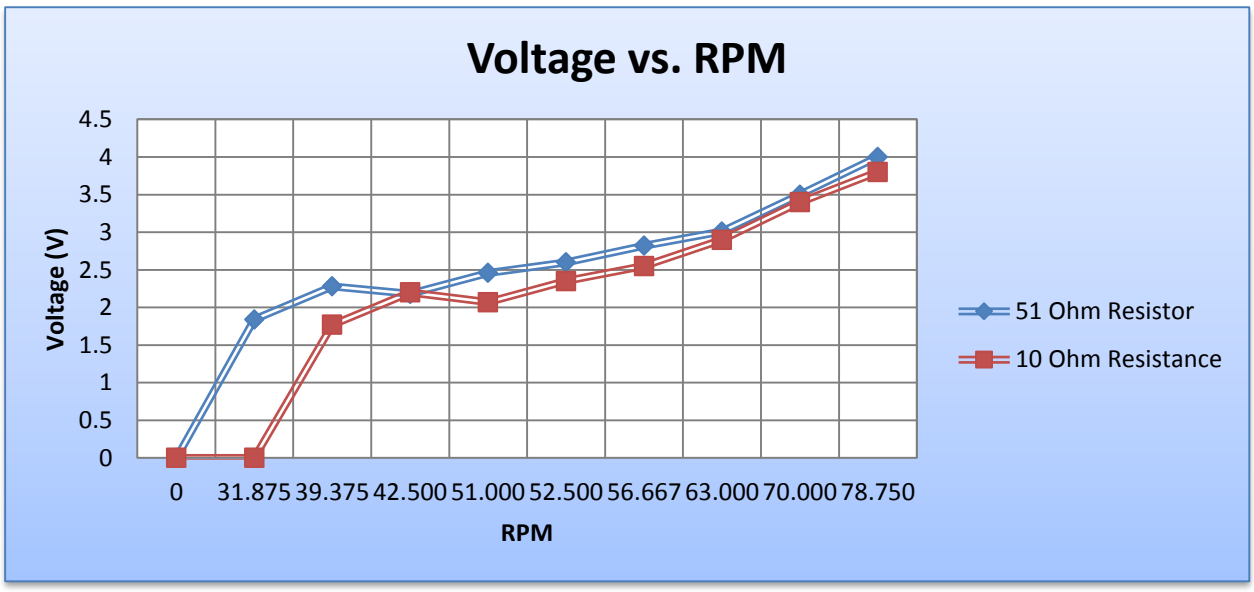

Figure 65: Voltage vs. Rotations per Minute (Dry Testing)

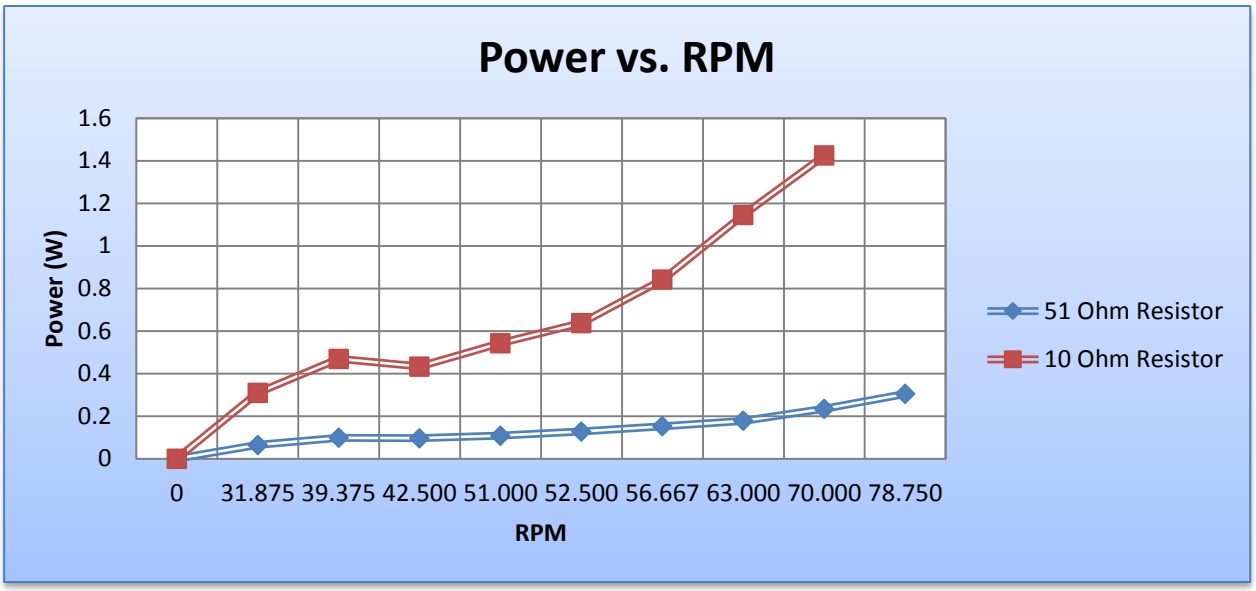

Figure 66: Power vs. Rotations per Minute (Dry Testing)

Figure 66, above, is a graph of power as a function of RPM. As expected, the output power increased with increasing RPM. The power generated across the smaller load resistance was also higher, as anticipated. As the resistance decreases, the current increases proportionally and if the current increases, power also increases. This can be derived from the following two equations:

$$V = I \times R$$

$$P = I \times V$$

In testing the alternator with the dry test device that was built, the highest achieved RPM was under 80. Having the capability to test the alternator at much higher speeds would provide a better understanding of the alternator properties. The increase in power should be exponentially growing, but due to the low RPM it may seem to look somewhat linear.

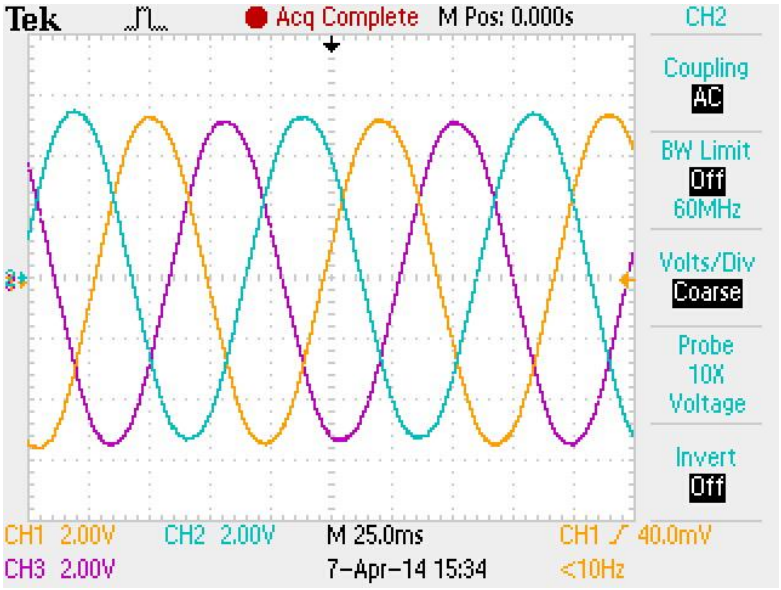

Figure 67: Three-Phase Voltage Waveform

The waveform in Figure 67 above shows the three-phase voltage output from the alternator during dry testing. Each voltage waveform is approximately 120° out of phase with each other waveform, as it should ideally be. The peak to peak voltage of each wave is approximately 10V.

CREW TANK TESTING RESULTS

The crew tank testing procedures took place over the course of three days. The average times for a 15ft float for 20Ω and 5Ω trails are listed in the tables below:

Table 7: Flume Speed Time Trials

Resistors at 20Ω					
Trial	Flume Times (s)				Ave (s)
1	4.78	4.78	4.81	4.26	4.6575
2	4.4	3.96	3.98	4.1	4.11
3	3.15	3.46	3.59	3.35	3.3875
4	3.11	3.25	3.04	3.21	3.1525
5	2.59	2.5	2.48	2.4	2.4925
6	2.23	2.05	2.05	2.2	2.1325
Resistors at 5Ω					
Trial	Flume Times (s)				Ave (s)
1	5.2	5	5.3	5.2	5.175
2	4.6	4.8	4.5	4.9	4.7
3	3.6	3.6	3.8	3.8	3.7
4	3.1	3.3	3.3	3.2	3.225
5	2.8	3	2.8	2.9	2.875
6	2.2	2.3	2.2	2.3	2.25

Using the time trial data from above, the flume speeds and corresponding results were recorded, as seen below:

Table 8: 20Ω Water Test Readings

Resistors at 20Ω					
Trial	Flume Speed (ft/s)	RPM	Voltage (V)	Current (A)	Power (W)
1	3.220611916	45.2	2.3	0.115	0.24
2	3.649635036	93	4.25	0.21	0.92
3	4.42804428	103	5.1	0.25	1.2
4	4.758128469	136	5.6	0.27	1.48
5	6.018054162	146	6.3	0.31	2
6	7.033997655	180	7.6	0.38	2.9

Table 9: 5Ω Water Test Readings

Resistors at 5Ω					
Trial	Flume Speed (ft/s)	RPM	Voltage (V)	Current (A)	Power (W)
1	2.898550725	30	1.2	0.25	0.3
2	3.191489362	43	2	0.35	0.7
3	4.054054054	82	3.5	0.65	2.3
4	4.651162791	110	4.6	0.88	4.1
5	5.217391304	125	5.2	1	5.3
6	6.666666667	150	6.4	1.2	8.5

The data from these tables is represented in the following three charts which depict the flume speed relationship to RPM for both resistances as well as the electrical characteristics (V, W, A) for the variety of RPMs. There was a significant increase in power and current when the resistors were lowered, which is the expected result from Ohm's law. While power and current changed between the trials, there was little change between the voltage values. This is due to the proportional relationship between induced voltage and frequency, which directly corresponds to RPMs.

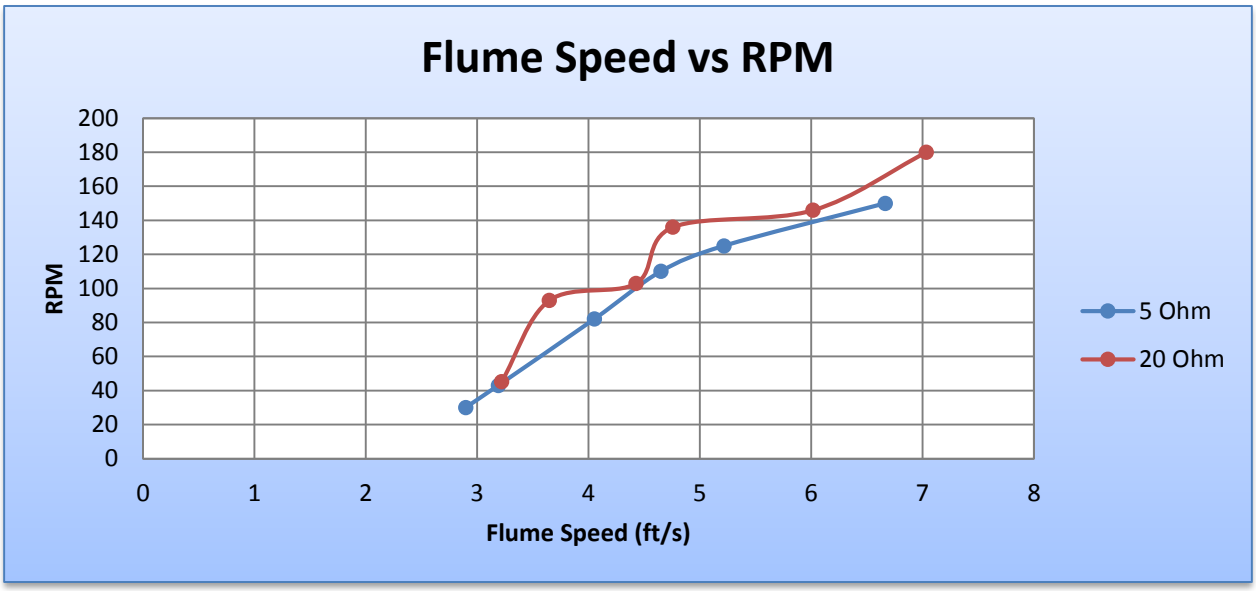

Figure 68: Flume Speed vs. RPM

As expected, Figure 68 shows that the RPM of the turbine increased proportionally with an increase in flume speed. Ideally, there should be no deviation in results since flume speed was not dependent on the resistance values being used. The discrepancy should be thought of as human error that could have been a result of how the flume speed data was collected. There is also the question as to how consistent the water flow generated by the crew tank was. Regardless, the differences in the graph are not essential to understanding how device RPM increases linearly with flume speed.

Below, Figure 69 and 70 show the electrical readings for water testing with a 20Ω and a 5Ω load configuration. As RPM increased, voltage and current increased linearly while power increased more exponentially. As with the dry testing, higher power output was achieved with the smaller load configuration.

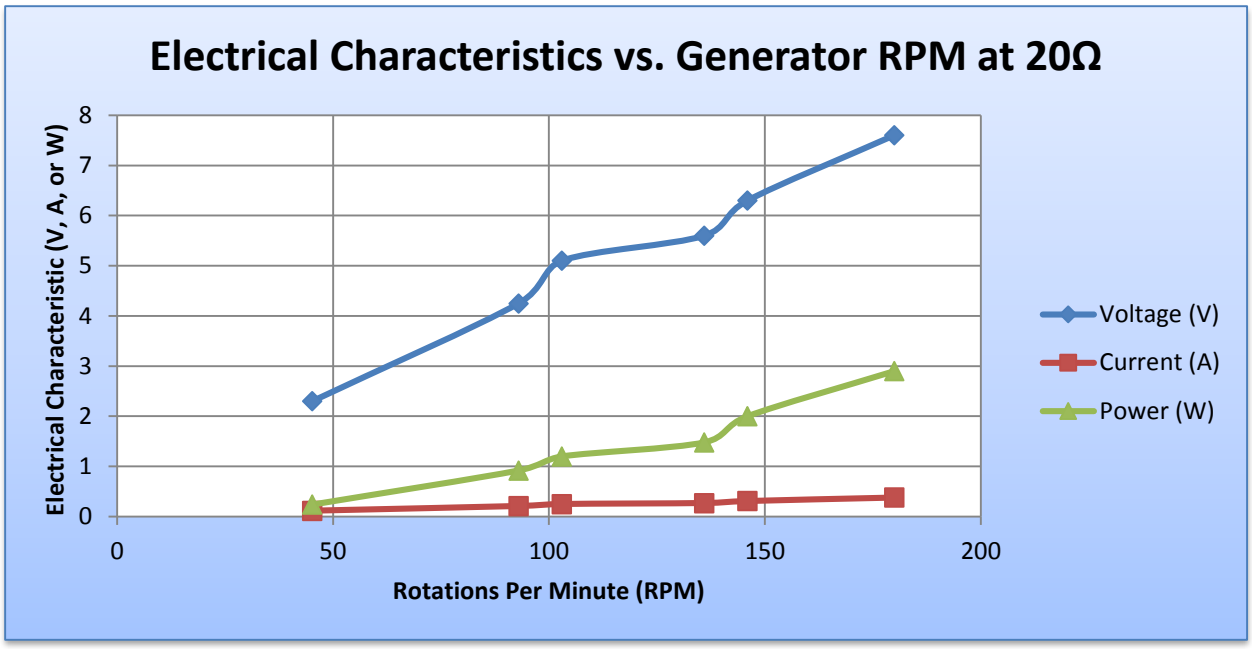

Figure 69: Power, Voltage, and Amperage vs. RPM for 20Ω Trials

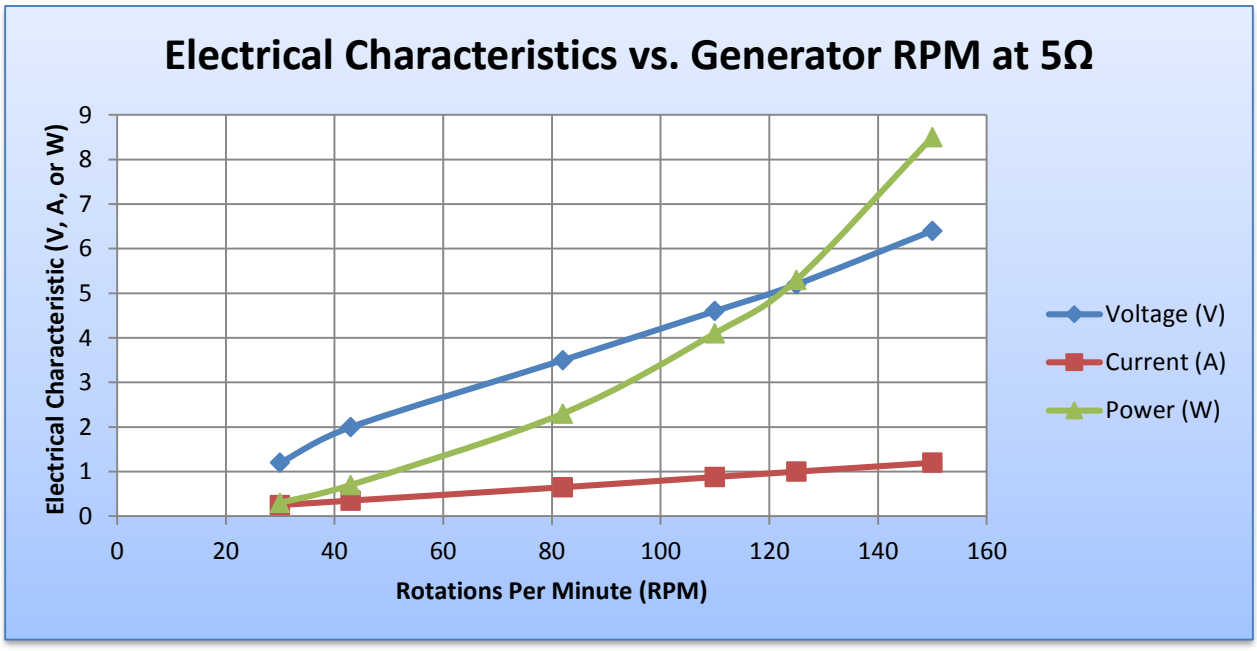

Figure 70: Power, Voltage, and Amperage vs. RPM for 5Ω Trials

CONCLUSIONS

Based on the information collected from the testing process, the group was able to draw several conclusions. First and foremost, the proof of concept was successful. The group was able to create a consistent sinusoidal three-phase AC voltage waveforms, proving the generator could create an adequate amount of power. However, the resulting output was not substantial enough power to effectively charge a battery. This is an area that requires further analysis and refinement. A potential drawback that the project team diagnosed was the difficulty associated with the production of a rotor-stator-rotor alternator. Component selection and tolerance was very important because minor changes could have been compounded to prevent full functionality.

Additionally it was evident that there was much difficulty in producing significant power with a small size generator utilizing a direct-drive alternator. The majority of devices that are employed for industrial applications utilize some form of gearbox to spin the alternator much faster than the turbine's blades. There was also problems with material selection for the prototype alternator that the group believes ultimately impacted performance. It was originally the group's intention to use M36 Non-Oriented Electrical Steel for both rotor plates but the parts did not arrive on time. This forced the group to order two back-up cores, which has a slightly higher resistivity than the electrical steel. If the M36 Non-Oriented Electrical Steel was utilized, we could expect to see less eddy current losses and a smaller deviation between the peak output amplitudes of the three-phase converter. This would have provided a cleaner and slightly stronger, more consistent electrical signal to work with.

Despite these drawbacks, the device still met many of the group's design specifications. The generator could fully function in an underwater environment without any damage to the internal parts or electronics. It was able to rotate in both the horizontal and vertical orientations, satisfying the requirement of bidirectional flow, and successfully capable out outputting three-phase power. It was a small, lightweight, scalable model that was both able to demonstrate its capabilities but also highlighted specific areas for improvement.

Several specific areas where the device was particularly successful or effective are present through its development. First, the production of the helical turbines using a MakerBot rapid prototype made the creation of consistent, twisting hydrofoil profiles much easier to create than through traditional methods. It also presented an

advantage in the budgeting of the project as its use of PLA is a low-cost, effective material for use in this scenario. The use of HDPE for the cross members was also exceptional in performance at this size. It was a very easy material to machine, remained strong when exposed to water and provided sufficient strength to stabilize the machine through the running currents. The axial flux alternator also proved to be a good choice as it was easier to manufacture and assemble than a traditional radial flux alternator would have been, while also providing the advantage of being flat and compact. The clips included on the ends of the machine would function well for the continued linking of the devices and also served well in the fixturing of the device in the testing environment.

The helical turbine functioned well in its usage of accepting multiple directions of inputs. The device was tested successfully both on its side and standing up. Additionally, the turbine was able to self-start, a predetermined key functionality of the design. Furthermore, the hydrofoil design was not independently evaluated but the relationships between flume speed and RPM indicate that the blades did produce positive lift and accelerated the turbine above a drag based speed.

Overall, the group is highly satisfied with the project and hopes that future endeavors will increase interest and investment in renewable marine current energy.

RECOMMENDATIONS

Based on the performance of the machine, the project team would make several recommendations relevant to the continued development of this machine. These changes include specific redesigns to the alternator and turbine, but also addresses the generator size and general material concerns. The group believes more can be done to overall improve machine design and efficiency.

The turbine blades performed effectively in the testing, however, the alternator would have benefitted from a higher RPM. Being limited by the 6ft/s maximum flume speed in the crew tank, the device never saw its full potential in a testing environment. Decreasing the solidity of the helical turbine would facilitate this in some way by increasing the tip speed of the machine. The aspect ratio, pitch and total size of the helical turbines could also be adjusted to varying successes. Also to ease manufacturing and add support, male-female assembly features should be integrated into the meeting faces of top and bottom blade halves.

As discussed above, the introduction of electrical steel into the alternator would provide a performance gain. Electrical steel contains precise laminations designed for use in motor and alternator applications such as an M36, 24 gauge, or C5A coated steel. These steels function by directing magnetic flux and are proven to provide a performance gain over traditional steels. The introduction of this new steel would drastically reduce changes in output amplitudes between the three-phases and would make DC rectification simpler.

Additionally, the introduction of a gearbox would increase the power output of the machine, this does however introduce complications such as placement and decreased efficiency as well as introducing potential problems related to gearbox failure. However, it would be useful in increasing output power.

To further increase efficiencies, the usage of a pre-purchased industrial underwater alternator would also make the machine more efficient. While the alternator built by hand for this project was successful and did produce energy as expected, inclusion of a professionally manufactured alternator would significantly raise the efficiency of the system. On a lesser scale, the adjustment or recreation of the existing alternator could be modified. In the stator design, this includes reducing the air gap size, adding cores to the coils, or increasing coil

sizes and number of turns. The air gap was nearly twice the value as expected, and the group believes the lack of a professionally manufactured alternator to be a principal reason why generator efficiency was lower than expected.

It would be beneficial to the project if the device were to be scaled up in size and tested in a larger underwater environment, such as the ocean or a river. This could include increasing the machine size as a whole, or select components in the attempt to prove the scalability of the project. However, there is still a risk associated with the lack of a controlled testing environment that might compromise the device. While this could be beyond the scope of a future MQP, it would provide useful feedback for the current design. If the project is continued, the group expects further design iterations to enhance performance.

REFERENCES

Linear Power Supply & Heat Sinks. (2007). Retrieved 2014, from University of Nevada, Las Vegas: http://www.physics.unlv.edu/~bill/PHYS483/power_supply_info.pdf

Cobscook Bay Tidal Energy Project. (2012, September 17). Retrieved from ORPC.com: http://www.orpc.co/newsevents_photogalleryDetails.aspx?Aid=7vWHuJea%2bLw%3d

Tribes. (2012). Retrieved 2014, from http://images.tribe.net/tribe/upload/photo/b2a/cf8/b2acf863-d73a-4b5c-b650-da80cc4eaa85

Microsun - Free Energy. (2013). Retrieved 2014, from Microsun - Free Energy: http://www.phemax.com/freeproject.html

Savonius Wind Turbines. (2014, January 14). Retrieved 2014, from REUK.co.uk: http://www.reuk.co.uk/Savonius-Wind-Turbines.htm

Aarchiba. (2007, June 21). *Darrieus Wind Turbine*. Retrieved 2013, from Wikipedia.org: http://en.wikipedia.org/wiki/File:Darrieus-windmill.jpg

Association, N. F. (2008). *Allowable ampacities of insulated conductors rated 0 through 2000 volts, 60°C through 90°C, not more than three current-carrying conductors in raceway, cable, or earth (directly buried) based on ambient temperature of 30°C.*

Basantani, M. (2008, March 19). *World's largest tidal power project coming to Korea*. Retrieved 2013, from Inhabit: http://inhabitat.com/worlds-largest-tidal-power-project-coming-by-2015/

Beckley, P. (1999). Modern Steels for Transformers and Machines. *Engineering Science and Education Journal*, 149.

Burman, Kari, & Walker. (2009). *Ocean Energy Technology Overview.* U.S. Department of Energy.

Caricchi, F., Crescimbini, F., Fedeli, E., & Noia, G. (1994). Design and Construction of a Wheel-Directly-Coupled Axial-Flux PM Motor Prototype for EVs. *Proceedings of 1994 IEEE Industry Applications Society Annual Meeting. 2*, pp. 254-261. Denver, CO: Industry Applications Society.

Chen, Y., & Pillay, P. (2005). Axial-flux PM Wind Generator with A Soft. *Industry Applications Conference: Fourtieth IAS Annual Meeting*, (pp. 231-237). Atlanta, GA.

Colton, J. L., Mularcik, B., Kennedy, B. J., Camilleri, S., & Rohoza, R. (2009). A comparison of radial and axial flux structures in electrical machines. *Electric Machines and Drives Conference*, 1029 - 1035.

Electronics, N. (2013, March 27). *Magnets: Samarium Cobalt vs Neodymium*. Retrieved 2013, from http://teamnovak.com/: http://teamnovak.com/tech_info/view_article/25

Energy, U. D. (2012, July 15). *Small Solar Electric Systems*. Retrieved March 19, 2014, from Energy.gov: http://www.energy.gov/energysaver/articles/small-solar-electric-systems

Gieras, J. F., Wang, R.-J., & Kamper, M. J. (2004). *Axial Flux Permanent Magnet Brushless Machines.* Norwell, MA, U.S.A: Norwell, MA.

Gorban', A., Gorlov, A., & Silantyev, V. M. (2001). Limits of the Turbine Efficiency. *Journal of Energy Resources Technology*, 311.

Gorlov, A. (1998). *Development of the helical reaction hydraulic turbine. Final technical report, July 1, 1996--June 30, 1998.* Technical Repoort, Northeaster University, Boston MA.

Helical Turbine. (n.d.). Retrieved 2013, from https://d2t1xqejof9utc.cloudfront.net/screenshots/pics/136a740b9aee71ae58bf570ad5409472/medium.JPG

H-Type Darrieus Turbine. (n.d.). Retrieved 2013, from elite.tugraz.at: http://www.elite.tugraz.at/Jungbauer/pics/Image250.gif

Magnetics, B. (n.d.). *Magnetic Materials*. Retrieved 2013, from http://www.bjamagnetics.com/index.html: http://www.bjamagnetics.com/html/magnetic_materials.html

Niblick, A. L. (2012). *Experimental and Analytical Study of Helical Cross-Flow Turbines for a Tidal Micropower Generation System.* Mechanical Engineering. Seattle: University of Washington.

Rovio, T., Vihriala, H., Soderlund, L., & Kriikka, J. (2014). *Axial and Radial Flux Generators in small-scale Wind Power Production.* Tampere, Finland: Institute of Electromagnetics, Pampere University of Technology.

Saslow, W. M. (2002). *Electricity, Magnetsism, and Light.* Amsterdam: Thompson Learning, INC.

Sastry, J. (2005). *Analysis and Control of an AC/DC PWM Rectifier - Assisted Induction Generator.* Tennessee Technological University.

Strous, T. D. (2010). *Design of a permanent magnet radial flux concentrated coil generator for a range extender application.*

Teslaco.com. (2011). *98% Efficient Single-Stage AC/DC Converter Topologies.* Power Electronics Europe.

Wang, R.-J., Kamper, M. J., Van der Westhuizen, K., & Gieras, J. F. (2005). Optimal Design of a Coreless Stator Axial Flux Permanent-Magnet Generator. *IEEE Transactions on Magnetics*, 55-64.

Wikimedia Foundation, I. (2004, August 10). *Rectifier*. Retrieved February 2014, from Wikipedia: The Free Encyclopedia: http://en.wikipedia.org/wiki/Rectifier

Yang, X. S. (2012, January 25). Hydrofoil optimization and experimental validation in helical vertical axis turbine for power generation from marine current. *Ocean Engineering, 42*, 35-46.